sustainability

MDPI

Article

Multi-Objective Techno-Economic Optimization of Design Parameters for Residential Buildings in Different Climate Zones

Muhammad Usman * and Georg Frey

Automation and Energy Systems, Saarland University, 66123 Saarbrücken, Germany; georg.frey@aut.uni-saarland.de

* Correspondence: muhammad.usman@aut.uni-saarland.de

Abstract: The comprehensive approach for a building envelope design involves building performance simulations, which are time-consuming and require knowledge of complicated processes. In addition, climate variation makes the selection of these parameters more complex. The paper aims to establish guidelines for determining a single-family household's unique optimal passive design in various climate zones worldwide. For this purpose, a bi-objective optimization is performed for twenty-four locations in twenty climates by coupling TRNSYS and a non-dominated sorting genetic algorithm (NSGA-III) using the Python program. The optimization process generates Pareto fronts of thermal load and investment cost to identify the optimum design options for the insulation level of the envelope, window aperture for passive cooling, window-to-wall ratio (WWR), shading fraction, radiation-based shading control, and building orientation. The goal is to find a feasible trade-off between thermal energy demand and the cost of thermal insulation. This is achieved using multi-criteria decision making (MCDM) through criteria importance using intercriteria correlation (CRITIC) and the technique for order preference by similarity to ideal solution (TOPSIS). The results demonstrate that an optimal envelope design remarkably improves the thermal load compared to the base case of previous envelope design practices. However, the weather conditions strongly influence the design parameters. The research findings set a benchmark for energy-efficient household envelopes in the investigated climates. The optimal solution sets also provide a criterion for selecting the ranges of envelope design parameters according to the space heating and cooling demands of the climate zone.

Keywords: residential building; building envelope; multi-objective genetic algorithm; TRNSYS; climate zone; multi-criteria decision making; CRITIC; TOPSIS

Citation: Usman, M.; Frey, G. Multi-Objective Techno-Economic Optimization of Design Parameters for Residential Buildings in Different Climate Zones. *Sustainability* **2022**, *14*, 65. https://doi.org/10.3390/su14010065

Academic Editors: Mitja Košir and Manoj Kumar Singh

Received: 25 November 2021
Accepted: 20 December 2021
Published: 22 December 2021

1. Introduction

Energy consumption in buildings accounts for a major part of the worldwide final energy use. The building sector consumes 30% of global energy use and produces 28% of global CO_2 emissions. Residential buildings alone account for 22% of total energy use [1,2]. The household sector in Asia has the maximum share of 35% in global building energy consumption. The European housing sector comes second and is responsible for approximately 28% of global energy use in residential buildings. The projected growth in households' energy consumption is 1.4% per year from 2018 to 2050 [3]. The worldwide energy usage of residential buildings increased by 30% from 1990 to 2014. In emerging economies, this increment was more than 50% during that period [4]. This growing energy demand and associated CO_2 emissions have led to new design approaches for energy conservation in buildings. Subsequently, energy-efficient buildings are recognized as a sustainable solution in reducing energy consumption and CO_2 emissions.

The thermal performance of the building envelope determines the energy consumption for thermal comfort, which has an explicit impact on the overall energy demand of the

buildings [5]. Therefore, employing an integrative approach in the architecture of building envelope at the preliminary design stage plays a critical role in improving the energy performance of buildings. Designers need comprehensive information of building performance and make decisions among a large number of design possibilities. It is asserted that operational cost, energy consumption, and overall performance of buildings are dependent on the early design approach [6]. In the preliminary design stage, the designer needs to consider building orientation, ventilation rate, air leakage, solar gain, window-to-wall ratio (WWR), window shading, and thermal mass, which impact the building performance collectively or independently [7,8]. Climate is another decisive element in the architectural design of buildings. The variation in climate conditions of different regions makes the design phase more diverse and complex. The design parameters' solution sets differ for each climate, and the energy-saving potential also changes likewise [9]. The heat gain from electrical appliances is also a critical parameter to evaluate thermal load in a simulated environment, particularly the cooling load. A realistic electric heat gain profile can help calculate the amount of heat to be removed from the building in summer [10] and avoid overheating in winter [11].

Although building envelope design is an imperative prospect in building performance, it is not an easy task due to the wide variety of passive measures. It is difficult to quantitatively analyze the building optimization problem using a traditional design approach. Researchers have coupled building simulation tools such as Ecotect, EnergyPlus, Doe-2, and TRNSYS (Transient Systems Simulation Program) with optimization algorithms to determine energy-efficient solutions [7,12]. Optimization algorithms explore design alternatives with desired outcomes, and make it possible to trade-off between objective functions concurrently with the provided constraints of the design variables [13]. Genetic algorithms are widely applied in building energy optimization problems [14–21]. A population-based metaheuristic genetic algorithm transforms the population under the explicit rule of survival of the fittest to reach a desired state of the objective functions. Genetic algorithms can deal with the non-linearity in the optimization of building performance, and they also explore the global optimum solution and do not limit to local optimal points [22].

Penna et al. [23] performed a three-objective optimization analysis on a single-family house in two different climate locations of Italy by using the Transient Systems Simulation Program (TRNSYS) and non-dominated sorting genetic algorithm (NSGA-II). The goal was to minimize the energy cost and discomfort hours, and maximize energy performance by insulation of the envelope, high performance window glazing, and replacement of HVAC equipment. An optimal cost solution could save more than 57% energy consumption for both locations. Rabani et al. [24] proposed an optimization scheme to automate the identification of the best-suited window configuration, envelope, shading system, and energy supply system on an office building in Norway. Ascione et al. [25] coupled Energy Plus with NSGA-II to optimize the architecture design of residential buildings in four cities of Spain (Mediterranean climate). Window dimensions, window shading, type of window glazing, and the type of walls and roofs were determined to trade-off between the heating and cooling demands of the building. Ferrara et al. [26] coupled the energy model of a nearly zero-energy French household with the acoustic model in MATLAB, and optimized the building through the particle swarm optimization (PSO) algorithm in GenOpt for energy, cost, and acoustic performance. A building simulation tool IDA-ICE was coupled with NSGA-II in GenOpt, and the findings of the study showed a decease up to 77% in energy use. The best performance was achieved with a shading device control based on solar radiation and indoor temperature. Chang et al. [27] developed a flexible multi-objective optimization framework to improve energy performance, thermal comfort, and reduce emissions and building costs while optimizing various envelope parameters. The framework was tested on four residential buildings in Tokyo to find out the retrofit area of the envelope for optimal performance.

Since multi-objective optimization produces a series of Pareto solutions, selecting the best one(s) is challenging. Thus, some studies implemented multi-criteria decision-

making (MCDM) techniques to rank the Pareto solutions and choose the best one(s). Delgarm et al. [28] optimized the building energy performance and indoor comfort using a multi-objective optimization technique and used the technique for order preference by similarity to ideal solution (TOPSIS) to choose the optimal solution from Pareto fronts. In a study [29], three MCDM methods, namely, Analytic Hierarchy Process (AHP), TOPSIS, and Choquet, were used to determine the ranking of different façade design alternatives. MCDM requires the assignment of appropriate weights to the performance criteria involved. The weighing process includes a pairwise comparison of attributes by the experts in the subjective method. On the other hand, objective weighting methods such as mean weight, entropy method, standard deviation, and criteria importance through intercriteria correlation (CRITIC) determine the weights based on the variation in the objectives in Pareto solutions [30]. There are studies in the literature that used CRITIC for weighing the attributes and TOPSIS for ranking of the energy system alternatives in combination with multi-objective optimization. C. Xu et al. [31] used an MCDM framework to optimize the capacity of a hybrid (wind/PV/hydrogen) energy system. The Pareto fronts for the three-objective optimization problem were generated using NSGA-II. The CRITIC technique was employed to assign weights to the objectives, followed by the TOPSIS method for ranking the hybrid energy system alternatives. M. Babatunde and D. Ighravwe [32] also used CRITIC and TOPSIS simultaneously to evaluate the techno-economic performance of six PV/wind/battery/diesel generator energy system alternatives. The results also identify the most and least important technical and economic criteria of a hybrid energy system. T. Salameh et al. [33] employed the MSCDM technique to optimize hybrid energy system alternatives. The authors used three weighing methods—no priority, entropy, and CRITIC—and the TOPSIS technique was used to decide the best solution from nine alternatives. Additionally, the reliability of TOPSIS was also asserted by other ranking methods, such as WASPA, MOORA, and EDAS.

Building performance is strongly influenced by the climate conditions and needs to be considered at the primary design stage. For this purpose, Zhao and Du [34] optimized the orientation, configuration of windows, and shading system of an office building in four different climates, from severe cold to hot, of China. It was concluded that the design parameters in those climates varied to achieve the desired energy and thermal comfort performances. The window materials and depth of the overhangs were different for the optimal case in hot and cold climates. The installation angle decreased from 110° in severe cold weather to 80° in hot weather. A study investigated the optimal passive design of a residential building in twenty-five different climates [35]. The authors investigated the effect of window blinds during daytime and the natural ventilation rates, air changes per hour (ACH) = 1 and 1.5, for passive cooling. They considered the envelope thermal transmittance, WWR of the facade, and windows glazing for efficient passive design, but limited the optimization process to only five values for each design parameter. The optimization results showed that the recommended thermal transmittance of the walls and roof are 0.2 W/m^2 K and 0.6 W/m^2 K in severe cold and hot climates, respectively. The WWR in cold climates reached 80% with the aim of reducing the heating load only. Natural ventilation significantly decreased the cooling load in hot climates and reduced the overheating hours in cold climates. Naji et al. [36] conducted performance evaluation of a double-story detached house of 214 m^2 area using TRNSYS, EnergyPlus, and an evolutionary algorithm (NSGA-II). The optimal values of envelope insulation thickness and area, glazing, and shading of windows were determined in eight different locations corresponding to tropical, temperate, and continental climates in Australia. The small window area characterized the optimal solutions for tropical, hot desert, and humid subtropical, while the larger window area was optimal in oceanic climates. Low insulation of the envelope was optimal in tropical, while a high insulation envelope was suitable for oceanic climates. A high level of south shading was required for tropical and hot deserts, whereas cold climates required a lower shading. Harkouss et al. [37] investigated the performance of multi-story apartment buildings in different cities of Lebanon and

France with the purpose to minimize the electricity demand of the building. A multi-objective building optimization tool (MOBO) was coupled with Energy Plus to optimize the insulation thickness of the envelope, window area and shading, type of window glazing, and heating/cooling set points. The performance analysis indicated that it is essential to minimize the building thermal load using passive strategies and a high-performance thermal envelope. The results showed that the thermal load was decreased in a range of 6.7–33.1% in different cities. Delgarm et al. [38] used Energy Plus and NSGA-II to optimize the building orientation, window area, and window shading of a single thermal zone in four climates of Iran, which resulted in a 23.8–42.2% decrease in total energy consumption. The optimal WWR was 0.26 in the city with higher HDD and 0.08 in the city with higher CDD. The orientation and overhand depth were almost the same in all cities.

The building design is traditionally based on expert opinion and lacks consideration of various design possibilities and multidisciplinary performance analysis. In most regions, building energy standards are established but contain limited information on building envelope components. Usually, those standards provide the allowable thermal resistance or transmittance of the envelope components and WWR in some cases [39–55]. The comprehensive design approach involves building performance simulations, which are time-consuming and require knowledge of complicated processes. In addition, climate variation makes the selection of these parameters more complex.

Previous studies have reported the optimization methods and solution sets for different building design parameters. Those studies mainly focus on optimizing individual or combinations of design parameters, such as envelope insulation, window area, window glazing, and window shading. On the other hand, design optimization is performed for a single climate or different climates of a particular region [24–27,29,38]. Some authors have conducted multi-climate optimization but with limited design options [23,34–36]. Further, very few studies consider multi-objective and multi-climate optimization followed by the MCDM for a single-family house by combining the envelope design parameters from the literature [28,37]. Many researchers have optimized building designs in different locations and reported energy savings in space heating and cooling loads. However, it is hard to find a study that demonstrates the variation in the optimal envelope parameters and the respective improvement in thermal demand in all major climates.

The present work aims to establish guidelines for determining the unique optimal passive design of a single-family household in various climate zones worldwide. This is accomplished by coupling a dynamic energy simulation tool (TRNSYS) and a Python-based multi-objective optimization algorithm (NSGA III). NSGA III produces the Pareto fronts between the cost of thermal insulation and annual thermal load. In the second stage, CRITIC is employed to determine the objectives' weights based on the objective data from the optimization process. Then the TOPSIS method is applied to identify the optimal solution from the Pareto front.

In this study, a wide range of architecture parameters, including insulation of envelope, passive cooling through windows, WWR, window shading fraction, radiation-based shading control, and orientation, are optimized to minimize the thermal energy demand in twenty climates from the Köppen–Geiger classification. This research contributes to scientific originality by identifying the household's optimal design parameters to efficiently achieve thermal comfort in various climates. A comparison of the annual thermal load is provided between the optimal envelope design from this study and the base-case building with previous design practices. Therefore, the novelty of this work is to provide the benchmarking of envelope design with climate adaptability, which overcomes the limitations of the case building performance model. Moreover, since the climate is changing for the last decades globally, the developed guidelines provide a criterion to modify the building design in the future. Finally, the findings of this work explain the variation in design parameters and thermal loads (solar gains, infiltration load, and transmission load) in the investigated climates.

2. Materials and Methods

The optimal design parameters were evaluated by a two-stage optimization method in this study. In the first stage, genetic algorithm NSGA-III was coupled with the building energy simulation tool TRNSYS to generate Pareto fronts by minimizing the thermal insulation expenses and annual thermal load of a single-family household. In the second stage, the CRITIC method was used to determine the weight of the objectives, while the TOPSIS approach was applied to select the unique optimal solution from Pareto solutions.

A comprehensive investigation of energy-efficient design options of the building envelope was carried out for the preliminary design stage. The ideal thermal energy need of the building was evaluated instead of the heating or cooling energy of a specific HVAC system. The thermal loads were calculated for achieving the room temperature (T_{room}), 20 °C and 25 °C in winter and summer, respectively, and relative humidity of 50% throughout the year. The predicted mean vote (PMV) value was calculated for these conditions as a measure of thermal comfort. The scheme of the optimization process is presented in Figure 1, and described in Sections 2.1–2.4.

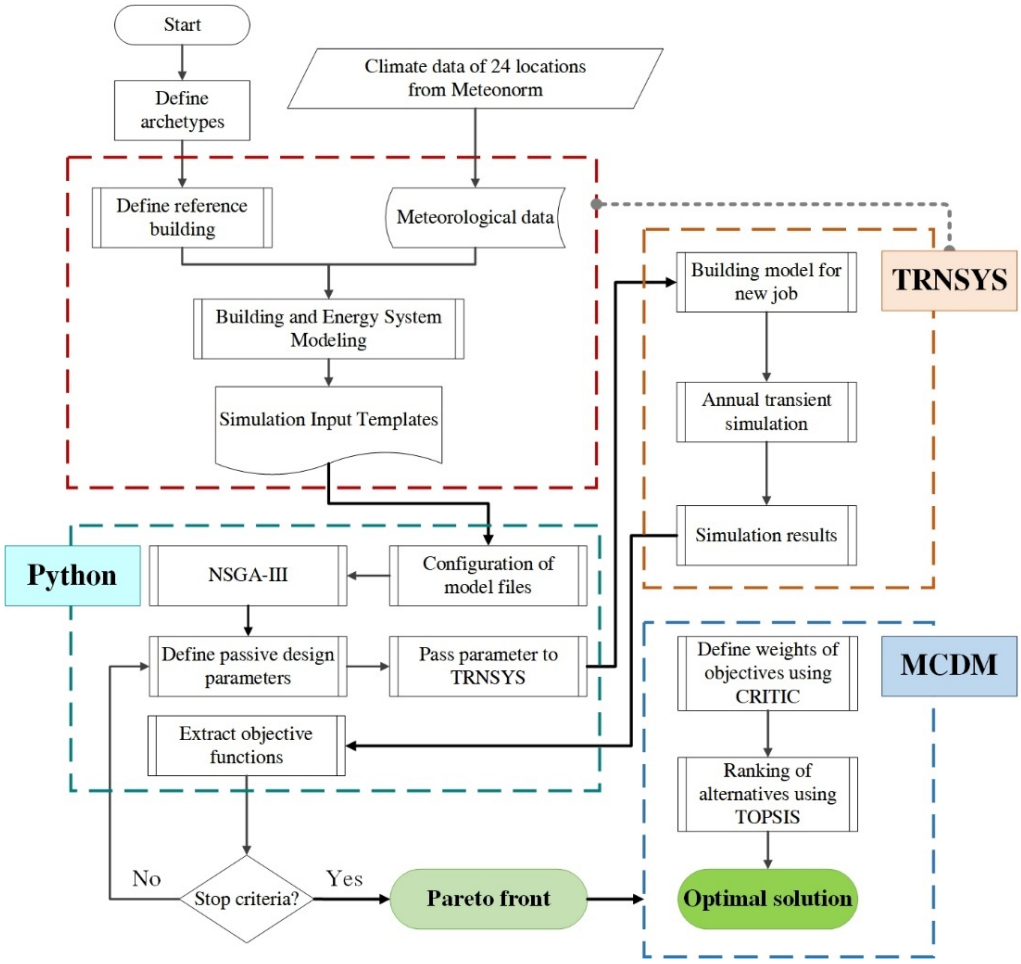

Figure 1. Python-based optimization scheme.

2.1. Base-Case Building

The base-case building model is a two-story residential building from International Energy Agency (IEA), Solar Heating and Cooling (SHC) Task 44/Annex 38 [56]. Building performance simulation was conducted using TRNSYS (Transient System Simulation Program) [57]. The building has a total net floor area of 140 m^2, an outside wall surface of 216 m^2, and an outer roof area of 81 m^2. Figure 2 shows the geometry and orientation of the building. The building was simulated as a single thermal zone. The internal walls (200 m^2)

and floor area of second story (70 m^2) were added in the TRNBuild tool to include the internal capacities of the building structure. The thermal properties of the envelope were defined based on the local building energy standards of each investigated location [39–55]. These standards provide the limits of thermal transmittance (U-value) for different components of the envelope. Tables 1 and 2 describe the construction and thermal properties of the building envelope. Expanded polystyrene (EPS) insulation and rockwool insulation layers were used for the external walls and roof, respectively. The thickness of the envelope insulation was defined such that the U-values of the external walls and roof met the criteria of allowed thermal transmittance in the local building energy standards. Double-glazed windows, having 4/16/4 geometry (4 mm inner pane, 16 mm space bar, and 4 mm outer pane), U-value of 1.4 W/m^2 K, and g-value of 0.622, were used for all facades.

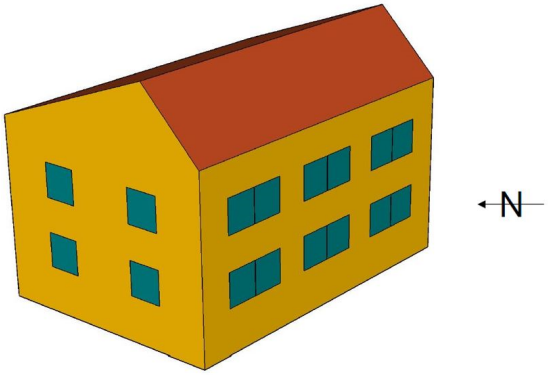

Figure 2. Geometry of the base-case building.

Table 1. Construction and thermal properties of the opaque elements.

Element	Layer	Thickness (m)	Density (kg/m^3)	Conductivity (W/mK)	U-Value (W/m^2 K)
External wall	plaster inside	0.015	1200	0.60	0.18 [1]
	brick	0.210	1380	0.70	0.16 [2]
	plaster outside	0.003	1800	0.70	0.20 [3]
	EPS (expanded polystyrene)	0.200 [1]	17	0.04	0.26 [4]
		0.230 [2]			0.30 [5]
		0.180 [3]			
		0.135 [4]			
		0.120 [5]			
Floor	wood	0.015	600	0.15	0.649
	plaster floor	0.080	2000	1.40	
	sound insulation	0.040	80	0.04	
	concrete	0.150	2000	1.33	
Roof ceiling	gypsum board	0.025	900	0.21	0.13 [1]
	plywood	0.015	300	0.08	0.17 [2]
	plywood	0.015	300	0.08	0.15 [3]
	rockwool	0.250 [1]	60	0.03	0.22 [4]
		0.190 [2]			0.20 [5]
		0.215 [3]			
		0.140 [4]			
		0.160 [5]			
Internal wall	clinker	0.200	650	0.230	0.885

[1] Ostersund and Stockholm; [2] Saarbrücken; [3] Strasbourg; [4] Milan; [5] All investigated locations other than mentioned earlier (c.f. Table 3).

Table 2. Construction and thermal properties of the windows.

Windows	Construction (mm)	Height (m)	Width (m)	Windows Area (m^2)	U-Value (W/m^2 K)	g-Value
North	(4,16,4)	1.0	1.0	3.0	1.4	0.622
South				12.0		
East				4.0		
West				4.0		

2.1.1. Ventilation Load

The energy performance analysis in this research takes account of two ventilation loads due to air exchange through the leakage area of the building and air exchange through windows opening. Based on the Sherman Grimsrud model from ASHRAE fundamentals 1997 [58], a simple single-zone approach calculates the air infiltration rate into the building through the leakage area (Equation (1)).

$$Q_{inf} = (A_L/1000) \cdot \sqrt{C_s \Delta T + C_w V^2} \quad (1)$$

where, Q_{inf} is the airflow rate (m^3/s), A_L is the effective air leakage area (cm^2) of the house, C_s is stack coefficient ($(L/s)^2/(cm^4\ K)$), ΔT is the difference between the average indoor and outdoor temperature for the time interval of calculation (K), C_w is wind coefficient ($(L/s)^2/(cm^4\ (m/s)^2)$, and V is average wind speed (m/s). The value of C_s depends on the number of stories of the building. For instance, it has a value of 0.000145 for a single-story, 0.00029 for a two-story, and 0.000435 for three-story buildings. The wind coefficient C_w depends on the height of the building and local shielding from surrounding objects, and the value is accordingly assigned as provided in ASHRAE fundamentals 1997.

The natural air exchange through six windows with aperture angle (α) is the passive cooling rate. Passive ventilation through windows was activated based on the indoor temperature of the zone and the ambient temperature (T_{amb}) during the night. Control strategies were implemented such that passive cooling through windows occurred during the night (9 p.m. to 8 p.m.) along with active cooling. The 24 h average temperature ($T_{avg}24$) was used to indicate the seasonal variation. It was asserted from the climate data set that the average temperature below 12 °C occurs in the winter season, and there is no requirement for cooling in the building. Passive cooling starts when the indoor temperature rises above 24 °C, and the outdoor temperature is at least 2 °C below the indoor temperature. In comparison, active cooling starts when the indoor temperature rises above 25 °C. The margin of 1 °C before the start of active cooling was provided as an energy-saving measure. When the room temperature drops to 23 °C, the windows are closed. Thus, the passive cooling is operable between 23 °C and 25 °C indoor temperatures. If all the conditions described in Figure 3 were met, the windows tilt to an angle α for passive cooling. Thus, the ventilation load of the building is a sum of the heat gains/losses from two air-exchange rates.

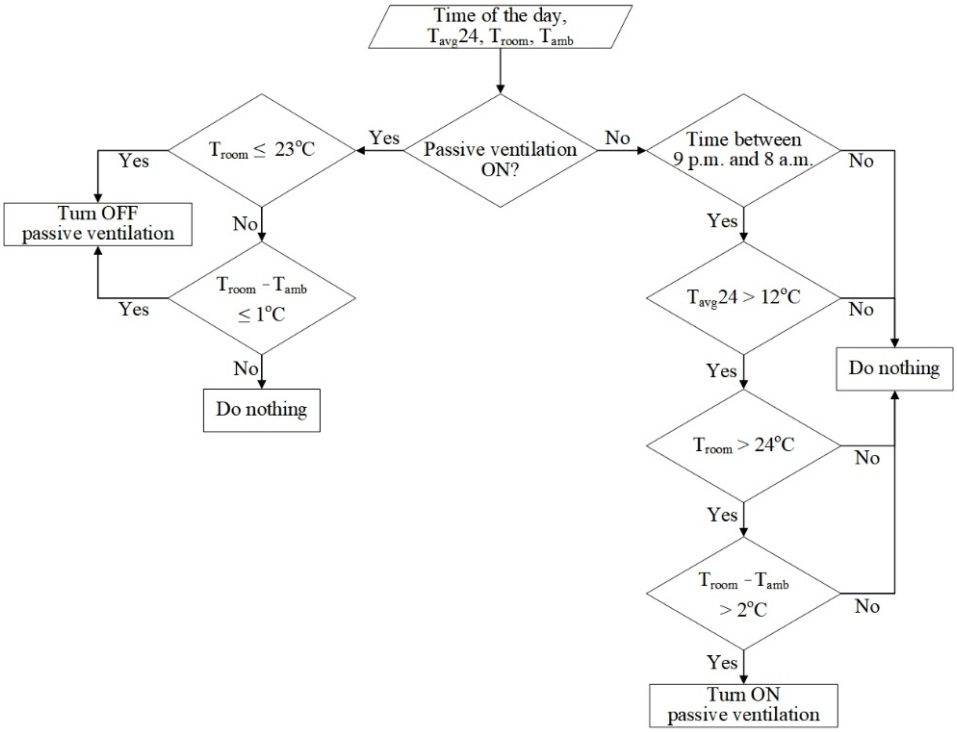

Figure 3. Temperature-based control of passive ventilation through windows.

2.1.2. Internal Gains

The investigated building was occupied by a family of four members. The occupancy schedule was adopted from ASHRAE [59], as shown in Figure 4, and is identical for all days of the week. The heat generated by the occupants is 115 W per person, which includes a sensible gain of 70 W and a latent gain of 45 W [60]. The sensible heat gain is divided into the radiative (42 W) and convective (28 W) parts. The latent heat is incorporated directly by the humidity with a mass flow of 0.059 kg/h.

Electrical appliances produce waste heat causing thermal gains in the zone. Since the electricity consumption varies with the diversity in the climate, annual hourly load profiles were generated based on the literature [61–75] for all the investigated countries to evaluate thermal gains. The load profiles do not include the electricity use for space heating, space cooling, and water heating. For realistic electric heat gains, the load profiles were modified, if required, to a household of 140 m^2 floor area. Kuusela et al. estimated the electricity consumption of common home appliances as a function of floor area. The relation between electricity consumption relative to a 140 m^2 household and floor area is shown in Figure 5 and mathematically represented in Equation (2) [76]. The electricity consumption of households in different locations was adjusted to a 140 m^2 floor area using Equation (2) because the area and geometry of the reference building were assumed to be identical for thermal load analysis in all climates.

$$y = -0.44\, ln(x) + 3.19 \quad (2)$$

It was assumed that 58% of the electric energy is retained in the building as thermal gain. Table 3 provides the electric gains in the selected climates. The occupancy and electric thermal gains were added as external hourly profiles to the building model in TRNSYS.

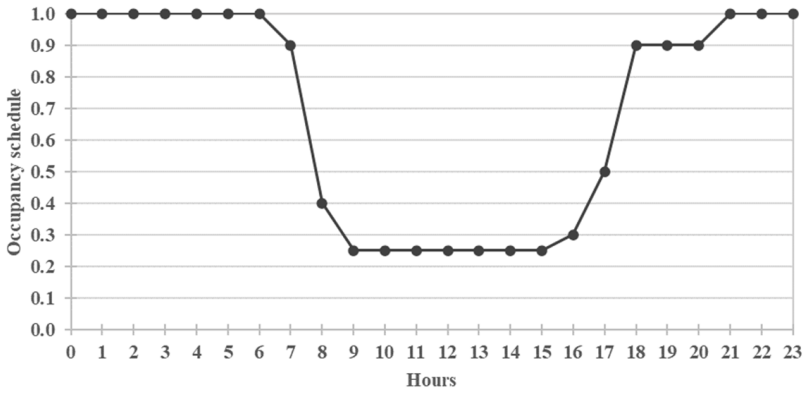

Figure 4. Occupancy schedule of a day from ASHRAE.

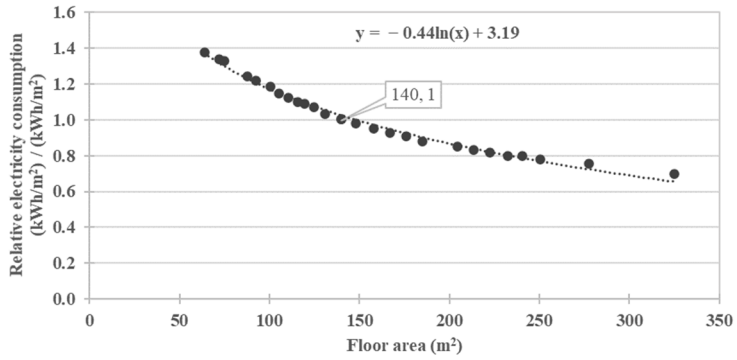

Figure 5. Relative electricity consumption as a function of area.

2.1.3. Solar Gain

All windows were equipped with shading blinds to avoid overheating in winter and higher cooling load in summer by limiting the solar gain. In this research work, a monthly schedule determined the shading fraction in the building model, and it was adjusted according to the month of the year, having the minimum shading fraction. According to a study, the average value of optimal shading during winter is approximately 23%, and the minimum value during a day is 10% [77]. In the summer season, the window shading can be varied between 25% and 100% for the optimization process [78]. Therefore, the minimum shading fraction is set to 0.11 in December for the base-case analysis. Figure 6 shows the variation in the shading for other months of the year relative to December. Furthermore, a windows-shading control was designed as a function of ambient temperature, the temperature of the zone, and global horizontal solar radiations. Figure 7 explains the control strategy to switch the shading device on and off. The temperature-based control of window shading restricts the solar heat gain into the building through windows. The window shade is turned on at 23.8 °C [56] to maintain the room temperature below 25 °C. This margin of 1.2 °C was used to delay the activation of the active cooling system. Although this value can be set to a lower level, it could result in higher lighting loads and heat gain from the lighting equipment. The window shading was turned off at 22.8, i.e., 1 °C lower than shading on temperature, to allow daylight into the building and avoid a further decrease in the temperature during summer. The WWR is the second factor that controls the solar gain through windows. WWR varies for all facades (c.f. Table 2), and the value of WWR is 20% for the south facade in the base case. For the optimization scheme, the upper limit of WWR is 40% according to the guideline of the ASHRAE standard 90.1–2019 [79], which states that the higher value of WWR is 40% for residential and non-residential buildings.

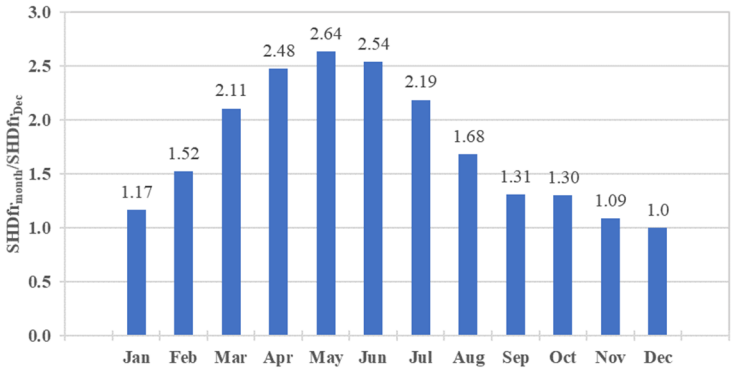

Figure 6. Relative shading fraction during the year.

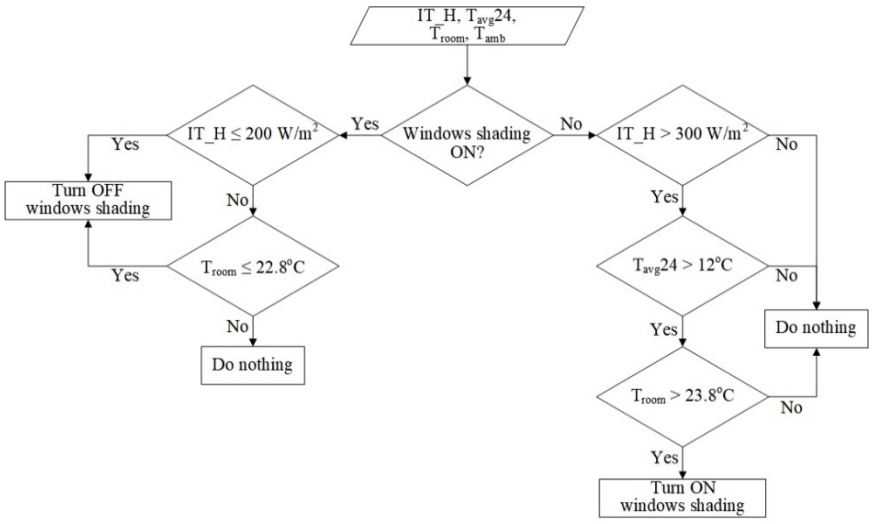

Figure 7. Solar radiation-based control of window shading.

2.2. Investigated Climates

This work investigated four major climate zones: A: Tropical; B: Dry; C: Temperate; and D: Continental, according to Köppen–Geiger climates classification [80] (first letter). These climate zones are subdivided based on the annual variation in ambient temperature and precipitation. The precipitation level (second letter) is defined as f (no dry season), m (Monsoon), s (dry summer), w (dry winter), S (semi-arid), and W (desert). Similarly, the temperature level (third letter) is categorized as a (hot summer), b (warm summer), c (cold summer), d (very cold winter), h (hot), and k (cold). Table 3 describes the average temperature (T_{avg}), cooling degree days (*CDD*), and heating degree days (*HDD*) for twenty selected climates of twenty-four locations. The Meteonorm tool generates the meteorological data for these locations. The CDD_{10} and HDD_{18} are defined as follows:

$$HDD_{18} = \sum_{t=1}^{365} (T_{base} - T_a) \quad (3)$$

$$CDD_{10} = \sum_{t=1}^{365} (T_a - T_{base}) \quad (4)$$

where T_{base} is 18 °C and 10 °C for *HDD* and *CDD*, respectively, T_a is the average temperature of the day, and degree days are the yearly sum of the daily temperature differences.

Table 3. Climate characteristics and electric gains of the investigated locations.

SN	Country	Location	Köppen Climate	IECC Climate	T_{avg} (°C)	HDD_{18}	CDD_{10}	Electricity Consumption (kWh/m^2 a)	Electric Gains (kW$_{th}$/m^2 a)
1	Sweden	Ostersund	Dfc	7 A	3.9	5468	429	30.20 [61]	17.52
2	Sweden	Stockholm	Dfb	5 A	7.4	3922	841	30.20 [61]	17.52
3	Austria	Bischofshofen	Dfb	5 A	8.3	3660	994	23.87 [62]	13.85
4	China	Daocheng	Dwb	6 A	5.9	4434	378	11.67 [68]	6.77
5	Iran	Sarab	Dsb	5 C	9.1	3496	1305	32.51 [69]	18.85
6	Japan	Sapporo	Dfa	5 A	9.3	3523	1430	28.80 [70]	16.71
7	China	Beijing	Dwa	4 B	12.8	2875	2470	11.67 [68]	6.77
8	Iran	Arak	Dsa	4 B	14.4	2320	2523	32.51 [69]	18.85
9	Denmark	Odense	Cfb	5 C	8.9	3364	835	26.77 [71]	15.53
10	Germany	Saarbrücken	Cfb	5 A	9.8	3119	1074	34.36 [62]	19.93
11	UK	Birmingham	Cfb	5 C	10.8	3679	930	37.34 [72]	21.66
12	France	Strasbourg	Cfb	4 A	12.1	2470	1533	30.00 [62]	17.40
13	China	Kunming	Cwb	3 C	15.7	1137	2204	11.67 [68]	6.77
14	Spain	Vigo	Csb	3 A	15.4	1282	2042	19.92 [73]	11.55
15	Italy	Milan	Cfa	4 A	13.9	2099	2115	21.81 [74]	12.65
16	China	Hanzhong	Cwa	3 A	15.4	1853	2589	11.67 [68]	6.77
17	Portugal	Evora	Csa	3 A	16.1	1404	2397	27.15 [75]	15.75
18	Iran	Birjand	BWk	3 B	17.0	1693	3052	32.51 [69]	18.85
19	Pakistan	Quetta	BSk	3 A	17.9	1182	3312	22.19 [63]	12.87
20	Pakistan	Lahore	Bsh	1 B	24.7	348	5382	22.19 [63]	12.87
21	UAE	Dubai	Bwh	0 B	28.9	0	6910	39.93 [64]	23.16
22	Singapore	Singapore	Af	0 A	28.6	0	6782	28.04 [65]	16.26
23	India	Mumbai	Aw	0 A	28.1	0	6594	22.92 [66]	13.30
24	Indonesia	Jakarta	Am	1 A	26.6	0	6045	18.40 [67]	10.67

2.3. Multi-Objective Optimization

TRNSYS is a stand-alone simulation program that calculates the thermal loads of the building and analyzes the performance of transient systems. TRNSYS uses text files as input to run the simulations and generates outputs also in text files. Python code devises an interface between TRNSYS and genetic algorithms to implement the multi-objective optimization process. This work used jMetalPy, an object-oriented Python-based framework, to solve the bi-objective optimization problem using a non-dominated sorting genetic algorithm (NSGA–III) [81]. The Python script reads the design variables and objective functions from the input and output files of TRNSYS, respectively, and formulates the optimization problem. jMetalPy generates a new set of design parameters for each simulation based on the values of objective functions from the previous run. Afterward, Python substitutes these values in the input files, and TRNSYS simulates the building energy behavior.

Multi-objective optimization results in a non-dominated solution set, called the Pareto front (PF), such that no other feasible solution exists that improves one objective without compromising the second objective.

2.3.1. Non-Dominated Sorting Genetic Algorithm (NSGA-III)

NSGA-III is an extension of NSGA-II and established as a baseline evolutionary multi-objective optimization algorithm. It uses several well-distributed reference points to select nondominated solutions for the next generation [82]. Thus, NSGA-III eliminates the drawback of non-diversity in NSGA-II during the generation of subsequent populations.

In the current optimization problem, NSGA-III carried out 5000 evaluations with a population size of 100 for each generation. Table 4 reports the input parameters for the bi-objective optimization process. The simulation-based optimization produced PFs of 100 non-dominated solutions for each location.

Table 4. Inputs of the genetic algorithm.

NSGA-III Attributes	Value
Population size	100
No of variables	7
No of objectives	2
Maximum evaluations	5000
Mutation method	Polynomial
Mutation probability	0.15
Crossover method	Simulated binary crossover
Crossover probability	0.8
Termination criteria	Max evaluations

2.3.2. Design Variables

The deciding factors of building thermal load are solar heat gains through windows, infiltration gains/losses through leakage area or the windows, and transmission gains/losses through opaque elements of the envelope. Therefore, the passive design parameters were selected based on their influence on heat gains and losses. The design variables for this study are building orientation, WWR, windows shading fraction, minimum solar radiation to turn on window shading, and the insulation thickness of the external walls and roof. Table 5 describes the detailed information of these variables.

Table 5. Design variables and their optimization bounds.

Building Element	Variable	Lower Bound	Upper Bound
External wall insulation	EPS thickness (EPS_{Thk}), m	0.10	0.25
Roof insulation	rockwool thickness ($Rockwool_{Thk}$), m	0.10	0.25
Window aperture	α (degrees)	5	20
South faced window	Window-to-Wall ratio (WWR)	0.2	0.4
Windows shading	Minimum horizontal solar radiation (IT_H) for shading on	250	500
Windows shading	Shading fraction in December (Shd_{Dec})	0.10	0.33
Building orientation	Orientation (N/S/E/W)	NA	NA

2.3.3. Objective Functions

The goal is to reduce the energy demand for heating and cooling by adopting passive design measures while keeping the investment cost to a minimum. Since this work deals with the passive design of the building, the optimization process only considered the additional cost for the envelope's insulation. TRNSYS computed the annual thermal load of the household using a multi-zone building component (Type 56). The building geometry, envelope materials, and the schemes of building gains/losses were defined in the TRNBuild tool and imported as a text file in the Type 56 component to run the simulation. TRNSYS also calculated the investment cost as a function of insulation thickness. The market survey of the envelope insulation material in different investigated locations revealed that the cost is approximately the same for the insulation materials, having similar thermal properties. The cost of EPS and rockwool materials were 139 €/m^3 and 230 €/m^3, respectively [83], and the same are used in all locations. Regarding the cost associated with the window area, it was assumed that the cost-saving from constructing a smaller size insulated wall compensates for the extra cost for large WWR. Finally, TRNSYS produced the values of the objective function in text files. The following two objectives come up for bi-objective optimization.

- Minimize annual thermal load (kW_{th}): The annual thermal load is the sum of sensible and latent heating and cooling demands to maintain the comfort level in the building. All the design parameters influence this objective function.

- Minimize investment cost (€): This objective function only depends on the thickness of insulation materials and is calculated accordingly.

2.4. Multi-Criteria Decision Making

The CRITIC method uses standard deviation to measure the diversity of the attributes. The method assigns weights such that the criterion with a higher diversity gets a higher weight. This process normalizes the data and creates a correlation matrix to measure the information and importance of each criterion (Equations (5)–(8)) [31].

$$r_{ij} = \frac{x_{ij} - x_j^{max}}{x_j^{max} - x_j^{min}} \tag{5}$$

$$r_{jk} = \frac{\sum_{i=1}^{m}(r_{ij} - \overline{r_j})\cdot(r_{ik} - \overline{r_k})}{\sqrt{\sum_{i=1}^{m}(r_{ij} - \overline{r_j})^2 \cdot \sum(r_{ik} - \overline{r_k})^2}} \tag{6}$$

$$c_j = \sigma_j \sum_{k=1}^{k} 1 - r_{jk} \tag{7}$$

$$w_j = \frac{c_j}{\sum_{j=1}^{n} c_j} \tag{8}$$

where r_{ij} is the normalized performance value of the ith alternative on the jth criterion, r_{jk} is the correlation coefficient between the j x k criteria matrix, σ_j is the standard deviation of the jth criterion, c_j represent the quantity of information contained in the jth criterion, and w_j is the weight of the jth criterion.

The TOPSIS method makes the ranking decision of the criteria based on the shortest and farthest geometrical distances of criteria from ideal and non-ideal solutions (Equations (9)–(13)) [31]. TOPSIS procedure was carried out by first determining the normalized values of the criteria in a decision matrix (Equation (9)). The normalization process was followed by the design of a weighted normalized matrix (Equation (10)). The weights obtained from the CRITIC methods were assigned here. The next step was to evaluate the distance of alternatives from ideal and non-ideal solutions (Equations (11) and (12)). Based on the outcomes of these equations, the relative closeness of the alternatives was calculated using Equation (13). The alternative with the highest score was considered the best solution.

$$n_{ij} = \frac{x_{ij}}{\sqrt{\sum_{j=1}^{n} x_{ij}^2}} \tag{9}$$

$$v_{ij} = \overline{n_{ij}}\cdot w_j \tag{10}$$

$$D_i^+ = \sqrt{\sum_{j=1}^{n}\left(v_{ij} - v_j^+\right)^2} \tag{11}$$

$$D_i^- = \sqrt{\sum_{j=1}^{n}\left(v_{ij} - v_j^-\right)^2} \tag{12}$$

$$D_i = \frac{D_i^-}{D_i^+ + D_i^-} \tag{13}$$

where n_{ij} represents the normalized value of the jth criterion for the ith alternative, w_j refers to the weight of the jth criterion, v_{ij} represents the weighted normalized value of the jth criterion for ith alternative, v_j^+ and v_j^- are the maximum and minimum values of the jth criterion, respectively, D_i^+ and D_i^- represent the ideal and non-ideal distances for the ith alternative, respectively, and D_i is the relative closeness of the ith alternative to the ideal solution.

3. Results

Firstly, the PFs are presented with trade-off solution points for all the investigated climates. The values of the design variables are provided along with the objective functions of the optimal solution. Secondly, thermal loads of the base-case and energy-optimal household models were extracted. The energy savings from the optimal passive design were also analyzed for heating and cooling loads. Finally, the variation in each design parameter with the changing climate was investigated.

3.1. Optimization Results

A multi-objective optimization does not produce a solution that minimizes or maximizes the objective functions simultaneously. Instead, it provides Pareto optimal solutions that are not affected by other solutions. Furthermore, no objective function can be improved without comprising at least another. The bi-objective optimization in this work generates the PFs for all the investigated climates with around 100 points. Figures 8–11 present the PFs of the continental, temperate, dry, and tropical climate zones, respectively. The 2D PFs plots between the cost of insulation and the annual thermal load were also drawn. The scatter plots are generally parallel in all climates. However, they are dispersed horizontally due to the diversity in climate conditions.

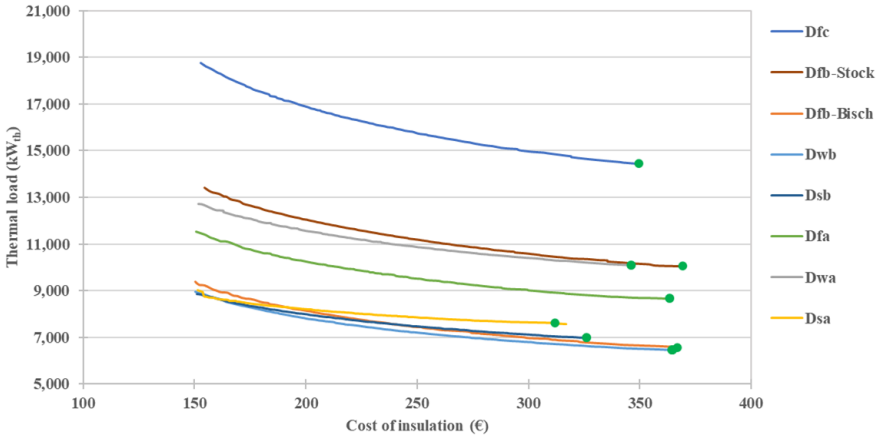

Figure 8. Pareto fronts of locations in a continental climate.

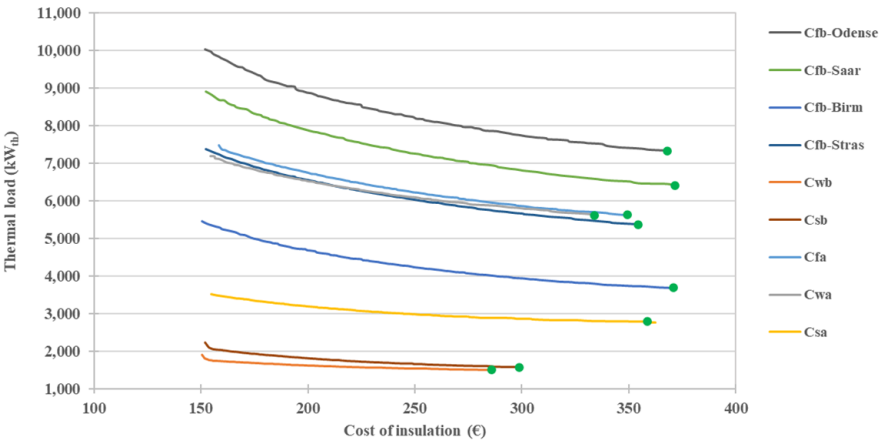

Figure 9. Pareto fronts of locations in a temperate climate.

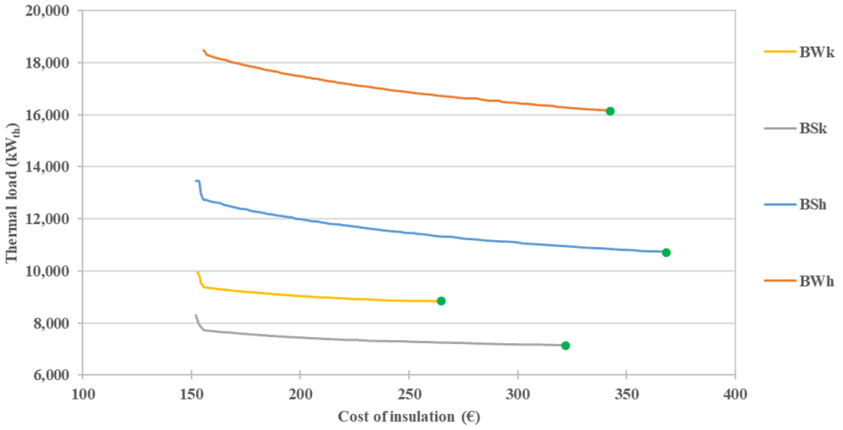

Figure 10. Pareto fronts of locations in a dry climate.

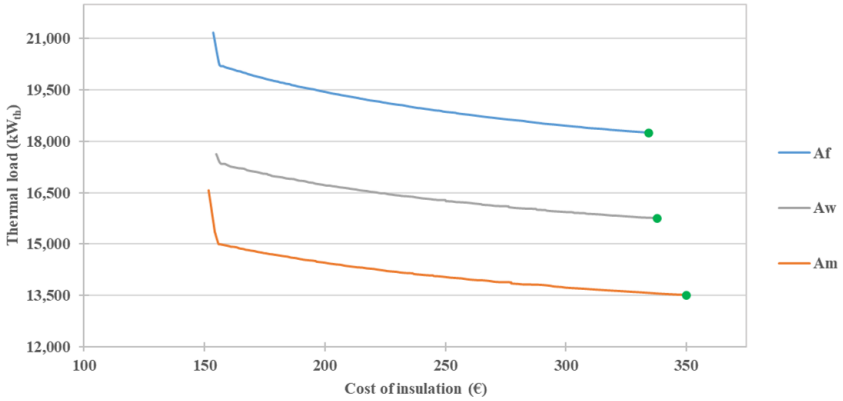

Figure 11. Pareto fronts of locations in a tropical climate.

The optimization results show that, initially, a minor increase in insulation cost results in a high reduction in the thermal load. This trend is more prominent in hot regions, as in the case of tropical and dry climate zones. In those climates, PFs are steeper at the start, but the slope gradually decreases as the cost of insulation increases. In this study, the optimum solution on a PF is determined by MCDM using the CRITIC and TOPSIS methods. The optimal solution is characterized by a low energy demand and high insulation thickness in all climate zones. The optimal trade-off solution is highlighted in green on PFs. It is interesting to note that the optimal solution is the one having the minimum thermal load or near to it in all cases. The phenomenon is justified by the higher weight obtained by the CRITIC method for the annual thermal load. In heating-dominant climates, the weight of thermal load ranges between 0.63 and 0.68, whereas this weight has a range of 0.60 to 0.72 in other climate zones.

Table 6 provides the values of design parameters, thermal transmittance of the external wall (U_w) and roof (U_r), and objective functions for the optimal solution in each location. In most cases, the optimal solutions require a highly insulated envelope and large window shading fraction. The WWR varies between the lower and upper bounds, i.e., 0.2 to 0.4. The solar radiation value remains near 250 W in most locations. Similarly, the average window aperture angle is 11.88 degrees but varies between 5 and 20 degrees in different climates. The U-value of the external wall and roof occurs around 0.15 W/m^2 K in climates with high space heating or cooling demand. However, it is relatively higher in moderate climates. In all cases, the U-value is decreased as compared to the base-case building after the optimization process other than Ostersund and Stockholm, where the U-value of the roof is increased from 0.13 W/m^2 K to 0.15 W/m^2 K.

Table 6. Trade-off solution set in the investigated climates.

Climate	EPS_{Thk} (m)	$Rockwool_{Thk}$ (m)	α (Degree)	WWR	IT_H (W)	Shd_{Dec}	Orientation	U_w (W/m^2 K)	U_r (W/m^2 K)	Thermal Load (kW$_{th}$/a)	Cost of Insulation (€)
Dfc (Ostersund)	0.247	0.211	9.8	0.37	279	0.330	North	0.150	0.154	14,317	350
Dfb (Stockholm)	0.237	0.196	10.9	0.31	289	0.330	North	0.156	0.164	10426	335
Dfb (Bischofshofen)	0.247	0.240	12.7	0.39	256	0.328	North	0.150	0.137	6729	367
Dwb (Daocheng)	0.245	0.241	5.2	0.40	287	0.253	North	0.151	0.136	6546	365
Dsb (Sarab)	0.234	0.188	11.0	0.33	255	0.329	North	0.157	0.170	7159	326
Dfa (Sapporo)	0.246	0.237	15.4	0.40	277	0.330	North	0.150	0.138	8845	364
Dwa (Beijing)	0.240	0.218	16.1	0.40	251	0.330	North	0.154	0.149	10,333	346
Dsa (Arak)	0.217	0.179	5.2	0.22	250	0.330	North	0.169	0.178	7757	317
Cfb (Odense)	0.246	0.237	10.0	0.34	304	0.328	North	0.150	0.138	7506	368
Cfb (Saarbrucken)	0.245	0.235	10.4	0.24	252	0.327	North	0.151	0.139	6595	372
Cfb (Birmingham)	0.240	0.249	13.1	0.32	279	0.329	North	0.154	0.132	3862	371
Cfb (Strasbourg)	0.244	0.214	12.3	0.28	260	0.330	North	0.151	0.152	5573	354
Cwb (Kunming)	0.160	0.219	7.3	0.22	250	0.330	North	0.222	0.148	1576	287
Csb (Vigo)	0.196	0.187	13.2	0.20	264	0.330	North	0.185	0.171	1674	298
Cfa (Milan)	0.231	0.223	16.1	0.28	251	0.330	North	0.159	0.146	5868	349
Cwa (Hanzhong)	0.232	0.203	8.4	0.32	255	0.328	North	0.159	0.159	5844	334
Csa (Evora)	0.235	0.224	19.2	0.20	261	0.330	North	0.157	0.145	2900	363
BWk (Birjand)	0.197	0.133	5.0	0.20	251	0.330	North	0.184	0.230	9000	265
BSk (Quetta)	0.223	0.185	12.0	0.20	250	0.330	North	0.165	0.173	7308	322
Bsh (Lahore)	0.249	0.219	16.3	0.20	256	0.330	South	0.149	0.148	10,826	368
Bwh (Dubai)	0.232	0.203	20.0	0.20	250	0.330	South	0.159	0.159	16,195	342
Af (Singapore)	0.250	0.167	13.4	0.20	251	0.330	South	0.148	0.189	17,933	334
Aw (Mumbai)	0.247	0.176	19.2	0.20	253	0.330	South	0.150	0.180	15,757	338
Am (Jakarta)	0.232	0.215	5.0	0.20	250	0.330	North	0.159	0.151	13,503	350

The variation in design parameters in the investigated locations can be characterized according to the degree days. The optimal solution sets are quite consistent in a specific range of degree days. Table 7 provides the mean, standard deviation (STD), and ranges in design parameters for climate zones having different degree days. The thermal transmittance should be low in heating-dominant locations. The mean value of thermal transmittance is the least in locations having $HDD_{18} > 3500$. The locations with $CDD_{10} > 3500$ have a mean thermal transmittance of 0.153 and 0.165 for the wall and roof, respectively. The WWR has a maximum mean value of 0.36 for $HDD_{18} > 3500$, decreasing to 0.2 for $CDD_{10} > 3500$. The window aperture angle has a mean value around 11 degrees for $HDD_{18} > 2000$. The maximum aperture angle occurs in locations having $CDD_{10} > 3500$, i.e., 14.77. For the horizontal solar radiation (IT_H), the mean value is maximum in the locations with $HDD_{18} > 3500$ and minimum in the locations with $CDD_{10} > 3500$. The STD is used to measure the spread of the solution set in different locations having similar climate conditions. The consistency of the solution sets is validated by very low STD in each category for all the design parameters, except for the aperture angle, which has a wide range and larger STD. A detailed analysis of variation in the design parameters for each climate zone is provided in Section 3.3.

Table 7. Comparison of the design parameters based on degree days.

Category		U_w (W/m^2 K)	U_r (W/m^2 K)	WWR	α (Degree)	IT_H (W)
$HDD_{18} > 3500$	Range	0.15–0.156	0.136–0.164	0.31–0.4	5.25–15.45	255–289
	Mean	0.152	0.144	0.362	11.192	278
	STD	0.003	0.013	0.040	3.505	11.90
$3500 > HDD_{18} > 2000$	Range	0.15–0.169	0.138–0.178	0.22–0.4	5.23–16.15	250–304
	Mean	0.156	0.153	0.297	11.599	261
	STD	0.007	0.015	0.061	3.789	19.62
$3500 > CDD_{10} > 2000$	Range	0.159–0.185	0.145–0.173	0.2–0.32	5.01–19.21	25–264
	Mean	0.179	0.171	0.224	10.859	255
	STD	0.024	0.031	0.048	5.083	6.04
$CDD_{10} > 3500$	Range	0.149–0.159	0.148–0.189	0.2	5–20	250–256
	Mean	0.153	0.165	0.201	14.772	252
	STD	0.006	0.018	0.001	6.042	2.65

3.2. Effect of Design Optimization on Thermal Loads

The optimization results reveal that energy-optimal solutions significantly reduce the space heating and cooling demand in all climates. The PMV index falls between −0.5 and 0.5 throughout the year for each case, which complies with the recommended thermal limit in ASHRAE standard 55 [84]. The design parameters change simultaneously during optimization until they reach an optimum solution. Therefore, it could be hard to understand precisely how an individual parameter influences the objective functions. Nevertheless, the overall effect of architectural design is evident by the improvement in the space heating and cooling demands. Building thermal loads includes infiltration losses/gains, transmission losses/gains, equipment gains, occupancy gain, solar gains, heating gains, and cooling losses. The passive design of the building is associated only with the energy transfer by infiltration, transmission, and solar radiation. Therefore, this work evaluates the variation in those thermal loads in the investigated climates, as shown in Figure 12. The clustered columns show the heat exchange for the base-case and optimal passive designs of the household, whereas the scatter plots represent the change in those thermal loads after optimization on the secondary vertical axis. The cumulative change in heat loss during winter and heat gain during summer is presented for transmission and infiltration loads. The optimization results show that envelope insulation, windows shading, and WWR are the most influential design factors for energy efficiency in households. In contrast, horizontal solar radiation for window shading control and window aperture (α) for passive ventilation do not significantly impact the thermal load.

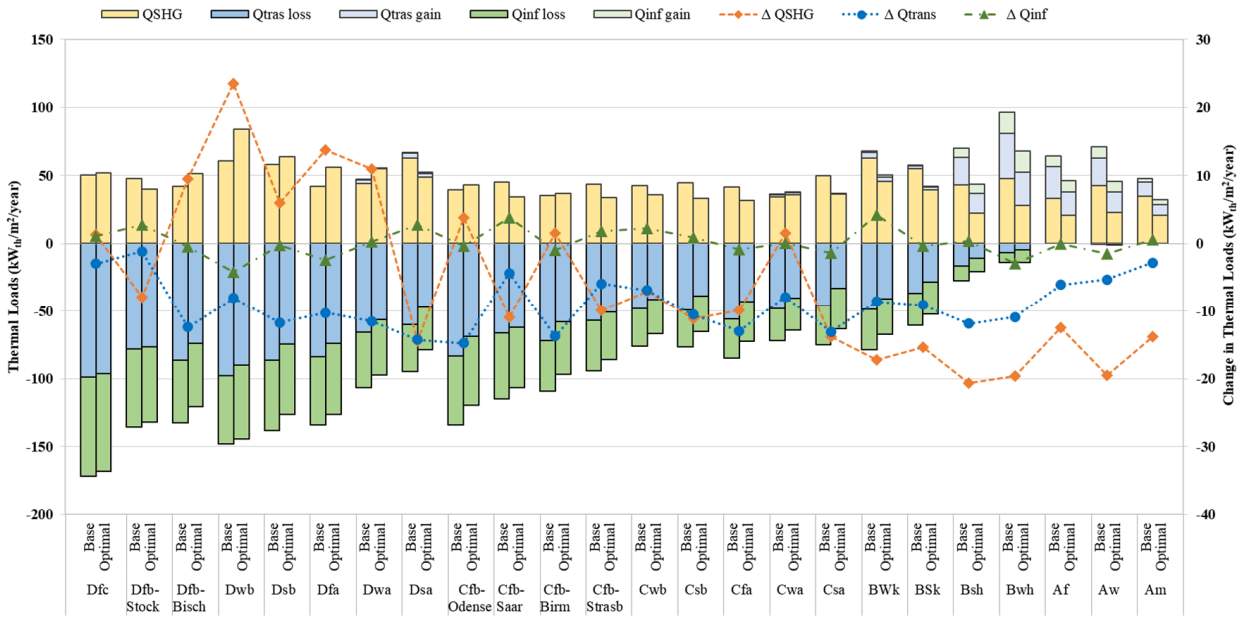

Figure 12. Households' thermal loads for the base-case and energy-optimal scenarios.

The optimal design increases the solar heat gains through windows (QSHG) in continental climates besides Dsa (Arak) and Dfb (Stockolm), whereas in temperate climates, solar gains slightly increase or decrease depending upon the space cooling demand of the location. In the case of tropical and dry climates, the QSHG is always reduced after optimization. Furthermore, the optimal passive design can decrease transmission losses during winter and transmission gains in summer. Thus, the net effect is lowering the transmission heat exchange (Qtrans) after optimization in all locations. The change in heat exchange due to infiltration (Qinf) is not very significant in cold and hot climates. Yet, it avoids overheating in winter or decreases cooling demand in summer to some extent through passive cooling. The following sections describe the improvement in energy demand of the household in four major climate zones of the Köppen–Geiger classification.

3.2.1. Continental Climate

The continental climate has the temperature of the coldest month below 0 °C and the temperature of the hottest month greater than 10 °C. Therefore, the locations in this zone are heating-dominant besides the hot and dry summer continental climate (Dsa). Even though the cooling energy demand is very low, the optimization further reduces it substantially. Figure 13 compares the heating and cooling energy demands of the base-case and optimal household and illustrates the energy saving after optimization. On average, the heating load decreases by 33.47%. The maximum reduction in heating demand is 56.93% in Dwb (Daocheng). In fact, the energy saving for space heating depends on the current practices of building energy standards. For example, after optimization, there is no significant change in the space heating loads in Dfc (Oestersund) and Dfb (Stockholm). This is due to the energy-efficient envelope standards in those locations.

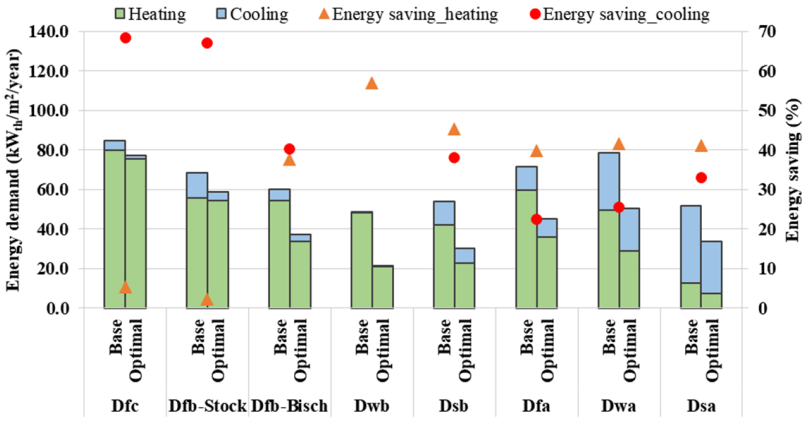

Figure 13. Heating and cooling loads and respective energy savings in a continental climate.

3.2.2. Temperate Climate

The temperate climate is characterized by the coldest month's average temperature between 0 °C and 18 °C and at least one month averaging above 10 °C. Figure 14 shows the energy demand of the base-case building and the energy demand and energy saving after optimization. The investigated locations show a mixed trend for space heating and cooling dominance. In contrast to the continental climate, the space cooling demand is relatively higher in temperate climates. The average energy savings for space heating and cooling are 33.36% and 50.98%, respectively. The energy saving is higher for lower energy demand and vice versa in both cases of heating and cooling. Therefore, a higher energy-saving potential in cooling load means these locations have lower cooling loads. Maximum heating demand and cooling demand, after optimization, are 42.59 kW_{th}/m^2 a in Cfb (Odense) and 18.54 kW_{th}/m^2 a in Cwa (Hanzhong), respectively.

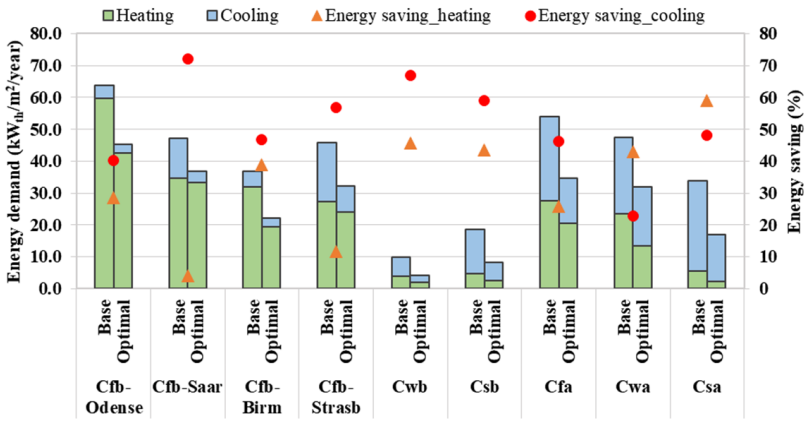

Figure 14. Heating and cooling loads and respective energy savings in a temperate climate.

3.2.3. Dry Climate

The dry climate is defined by very little precipitation during the year. Moreover, it has two subgroups based on the mean average temperature: hot, MAT $\geq$ 18 °C; and cold, MAT < 18 °C. Consequently, the locations in this zone have a long summer season and shortened winter season. The design optimization is equally effective in cooling-dominant climates, as shown in Figure 15. The energy saving in dry climates averages 33.3% for space cooling. Maximum cooling demand is 142.34 kW_{th}/m^2 a in the hot desert climate (BWh) of Dubai, which reduces to 99.45 kW_{th}/m^2 a after optimization.

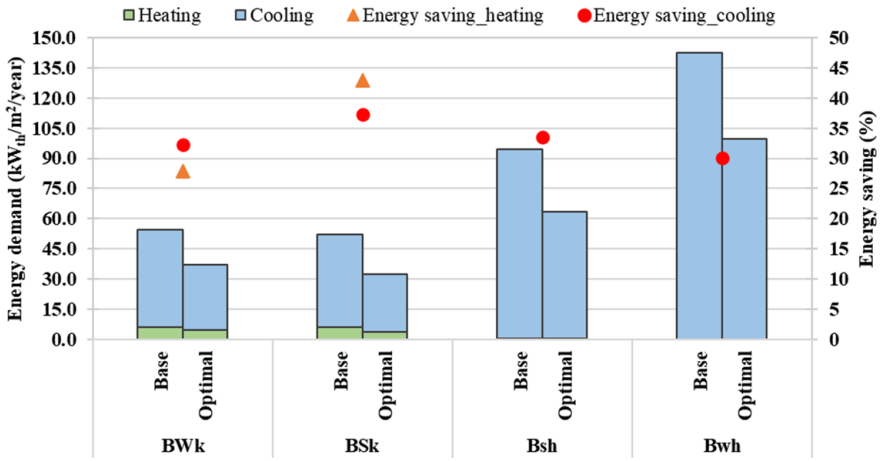

Figure 15. Heating and cooling loads and respective energy savings in a dry climate.

3.2.4. Tropical Climate

In a tropical climate, the average temperature of every month is 18 °C or higher, with significant year-round precipitation. The high humidity level throughout the year is another prominent feature of this climate. Therefore, there is no space-heating load in this climate, or it is so low as to be considered negligible. The space-cooling loads for three representative tropical climates and energy saving through design optimization are presented in Figure 16. The space cooling demand in Jakarta's tropical-monsoon climate (Am) is the lowest due to the higher precipitation. The highest energy saving is 29.4% in Mumbai, a tropical savanna climate (Aw). The average energy saving amounts to 25.95%, much lower than the heating-dominant continental and temperate climates.

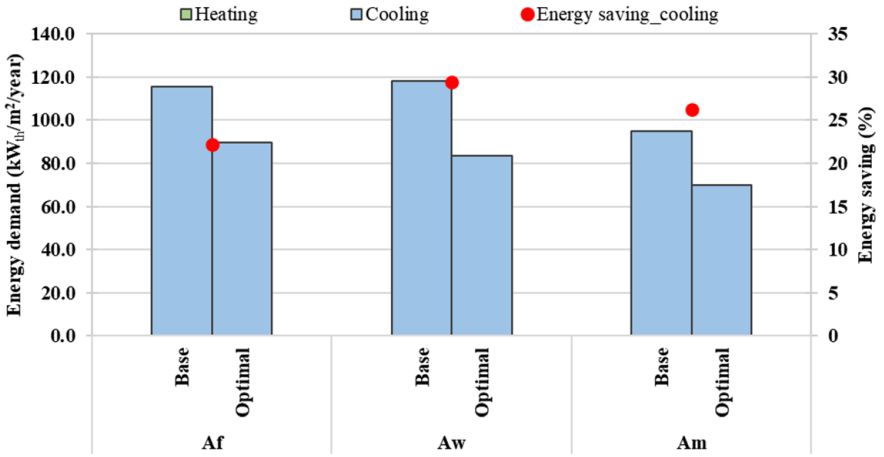

Figure 16. Heating and cooling loads and respective energy savings in a tropical climate.

3.3. Climatic Variation of Design Parameters

The optimization results show that the climate conditions significantly influence design parameters. Although each investigated climate requires a specific set of design parameters, the locations with similar climate conditions can be grouped to devise a climate adaptability pattern. Thus, the investigated climates were further categorized, as described in Table 8. The variation in each design parameter in the major climates zones is described in Sections 3.3.1–3.3.7.

Table 8. Categorization of the investigated climates.

Category	Climates
Continental—cold	Dfc
Continental—warm summer	Dfb, Dwb, Dsb
Continental—hot summer	Dfa, Dwa, Dsa
Temperate—warm summer	Cfb, Cwb, Csb
Temperate—hot summer	Cfa, Cwa, Csa
Dry—cold	BWk, BSk
Dry—hot	Bwh, Bsh
Tropical	Af, Am, Aw

3.3.1. External Wall Insulation

In general, the locations with extreme weather conditions have very insulated envelope to minimize transmission gains or losses. Figure 17 shows box plots of the change in the EPS thickness in different climates. The EPS thickness of the external wall is maximum, 0.247 m, in the continental—cold climate. It decreases to the mean value of 0.222 m in the temperate—warm climate because of the decreasing heating loads. In a temperate—hot climate, it is necessary to apply a higher level of insulation due to the significant cooling load. The dry—hot and tropical climates are cooling-dominant climates and require a larger insulation thickness of the external walls. Dry—cold climate has the lowest mean EPS thickness of 0.21 m, due to its lower space-heating and cooling loads than other climates.

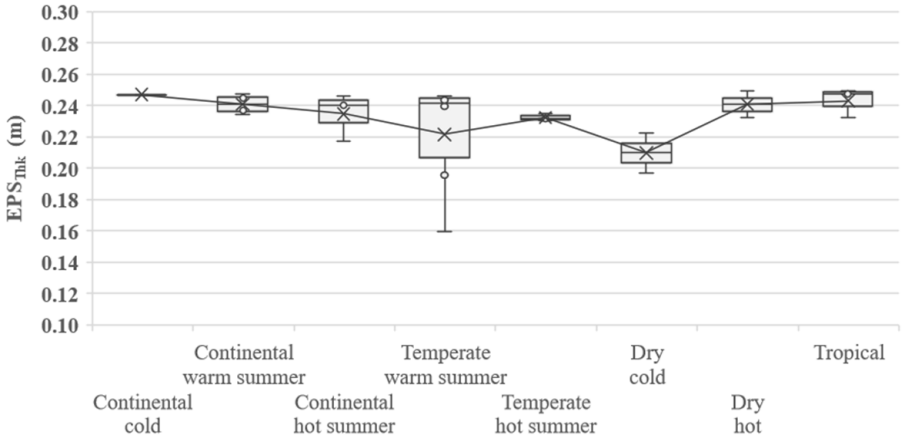

Figure 17. Variation in thickness of EPS insulation with climate.

3.3.2. Roof Insulation

The optimum solutions show that the insulation thickness of the roof is also higher than the base-case value in most of the climates, as illustrated in Figure 18. Though, it is lower than the EPS thickness of the external walls due to lower thermal conductivity of the rockwool material. The heating load of the location characterizes the rockwool thickness of the roof. Therefore, the roof has a higher rockwool thickness in continental and temperate climates than in dry and tropical climates. The heating load of hot summer climates is lower than warm summer climates. As a result, warm summer locations require larger insulation than the hot summer in continental and temperate climates. Similar to the EPS insulation for the external wall, the dry—cold climate has the minimum mean rockwool thickness of 0.159 m.

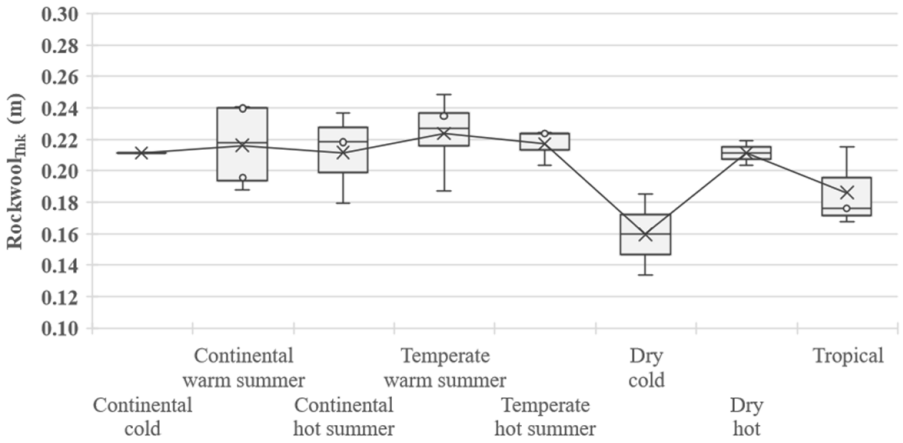

Figure 18. Variation in thickness of rockwool insulation with climate.

3.3.3. Window Aperture Angle

Figure 19 shows the variation in the optimal window aperture angle with changing climates. Since infiltration through window opening is active only for passive cooling, the aperture angle is more significant in hot climates. The aperture angle is higher in hot regions of continental, temperate, and dry climates. The dry—hot zone has a maximum mean aperture angle of 18.14 degrees. Although the dominant thermal load is cooling in a tropical climate, it also has a higher humidity level throughout the year. As a result, the aperture angle is relatively lower than the dry climate, and it even reduces to 5 degrees in Jakarta, a tropical-monsoon region. The dry—cold zone has the minimum aperture angle compared to other climate zones.

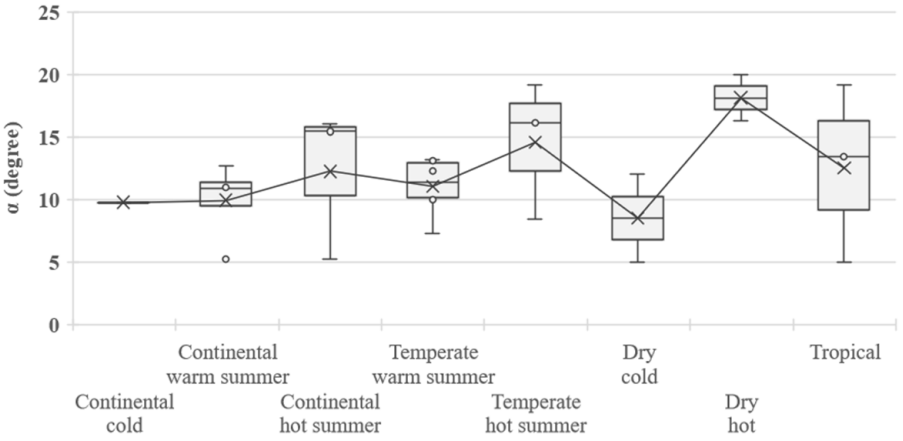

Figure 19. Variation in window aperture angle with climate.

3.3.4. Window-to-Wall Ratio

WWR is the most imperative element regarding the solar gains in both climates, heating-dominant or cooling-dominant. The box plots of WWR in different climate zones are presented in Figure 20. In general, the optimal solutions ascertain that the heating-dominant regions require higher WWR to maximize the solar gains. Therefore, the continental—cold climate has the maximum WWR, 0.37, continuously decreasing to the mean WWR of 0.27 in the temperate—hot summer climate. On the other hand, in the dry and tropical zone, the goal is to reduce the heat gains of solar radiation. Consequently, the WWR equals 0.2, the lower bound, in optimum solutions.

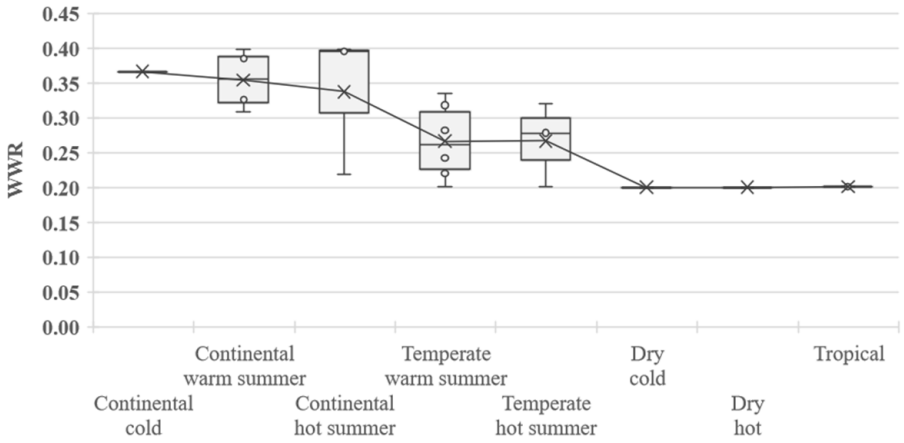

Figure 20. Variation in WWR with climate.

3.3.5. Solar Radiation for Shading Control

Minimum solar radiation to activate the window shading is another factor to control the solar gains into the household. Figure 21 shows the box plot of IT_H in different climate zones. This value is relatively higher in continental and temperate climates because the dominant thermal load is heating. The continental—cold climate has the maximum value of 279 W for IT_H. On the other hand, window shading activates at low solar radiation, around 250 W, in dry and tropical climates due to high cooling loads.

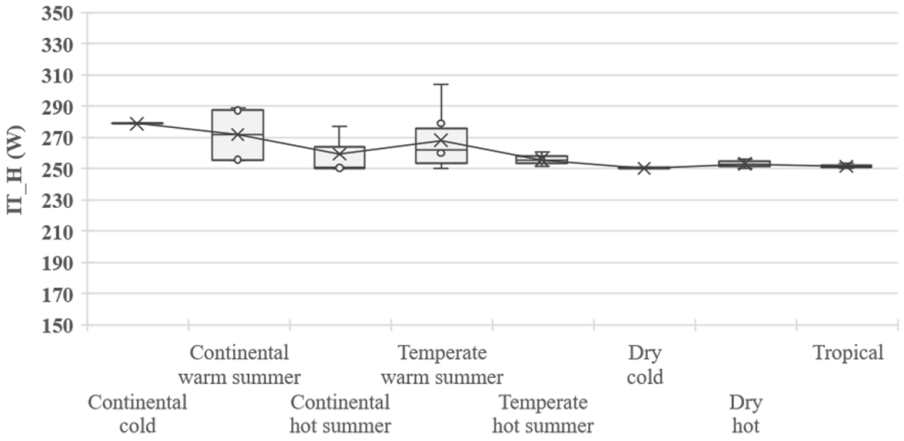

Figure 21. Variation in solar radiation for shading control with climate.

3.3.6. Window Shading Fraction

This study considers the shading fraction as a function of shading in December, the month of minimum shading fraction, as presented in Figure 6. To minimize the solar gains during summer, the optimal shading fraction in December remains close to the upper bound. Since the cooling load in Dwb (Daocheng) is negligible, the window shading fraction in December (Shd_{Dec}) drops to 0.253. For all other locations, it is above 0.326. On average, the shading fraction is 0.326 in December and 0.86 in May.

3.3.7. Building Orientation

The building orientation strongly influences the solar gains. Optimization results show that South or North is the optimal orientation in all climates. In most of the locations, the front facade is facing North, as shown in Figure 22. However, the locations in dry and temperate climate zones with minimal heating load have a South-facing optimal building orientation. The optimal orientation is an essential aspect of the building architecture since it increases energy efficiency without additional investment costs. It should be noted

that all investigated climates are in the Northern hemisphere. Therefore, these results are only applicable for households having an architecture similar to the case building in the Northern hemisphere.

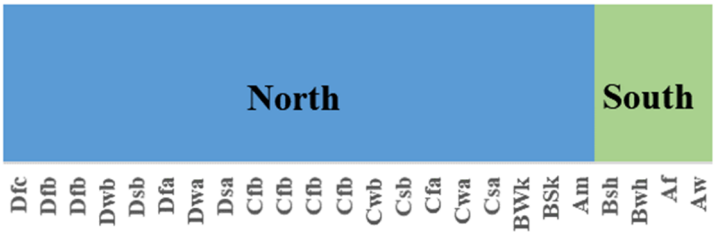

Figure 22. Optimal household orientation in the investigated climates.

4. Discussion

The bi-objective optimization poses two areas of discussion about the architectural design in different climate zones: energy saving in annual thermal load and the optimal design parameters.

For the case of energy saving through optimization, the continental—warm summer and continental—hot summer zones show 37.8% and 35.8% improvement on average in the annual thermal load, respectively. The temperate climate zone has the average energy-saving potential of 39.17% in warm summer regions and 39.51% in hot summer regions. This energy saving is higher due to the lower heating demand as compared to the continental climate. The design optimization more effectively restricts the transmission losses or gains in the heating-dominant climates. Therefore, energy saving decreases with the increased cooling demand. As a result, energy saving reduces to 34.8% and 31.6% in dry—cold and dry—hot climate zones. The tropical climate zone has the minimum energy saving of 26% in annual thermal load. Interestingly, the design optimization would also have a significant impact on the operational cost of the building. Since the optimization process shows a substantial improvement in the energy performance of the building, it would also decrease the operating cost compared to the base-case building. The operating cost of a building depends upon the type of equipment, energy-supply system, and local energy prices. Thus, the monetary savings from design optimization varies in each location. The current optimization process does not account for the cost of building operation, which is a limitation of this work.

With regard to the design parameters, Table 9 provides a criterion for selecting the energy-optimal ranges according to the climate zone and respective degree days. Although this criterion is based on the investigation of 24 cities in major climate zones, its legitimacy is asserted by achieving the optimal solution after a large number of simulations, i.e., 5000, in each location. However, the adaption of individual parameters is not advised because the design variables are strongly reliant on each other.

The continental—cold climate is represented by maximum HDD. So, it needs a high EPS thickness of 0.247 and rockwool thickness of 0.211, resulting in a low thermal transmittance of 0.15 W/m^2 K for the envelope. It is also characterized by large WWR, IT_H, and ShdDec. The continental—warm and continental—hot climates show a similar pattern for design variables, but their ranges drop with a decrease in HDD and increase in CDD. Furthermore, the window aperture angle needs to be increased from the continental—cold to continental—hot climate. Regarding the orientation, a North-facing household is the optimum choice in the continental climate zone.

Table 9. Ranges of optimal design parameters and degree days in different climate zones.

	Continental			Temperate		Dry		Tropical	
	Cold	**Warm Summer**	**Hot Summer**	**Warm Summer**	**Hot Summer**	**Cold**	**Hot**	**Rainforest/ Savanna**	**Monsoon**
HDD18	5468	3496–3922	2320–3523	1137–3364	1404–2099	1182–1693	0–348	0	0
CDD10	429	378–1305	1430–2523	835–2204	2115–2589	3052–3312	5382–6910	6594–6782	6045
EPS_{Thk} (m)	0.247	0.234–0.247	0.216–0.245	0.160–0.246	0.231–0.238	0.197–0.223	0.232–0.249	0.247–0.25	0.232
$Rockwool_{Thk}$ (m)	0.211	0.188–0.241	0.187–0.239	0.187–0.249	0.203–0.227	0.133–0.185	0.203–0.219	0.167–1.176	0.215
U_w (W/m^2 K)	0.15	0.150–0.157	0.150–0.169	0.150–0.222	0.157–0.159	0.165–0.184	0.149–0.159	0.148–0.150	0.159
U_r (W/m^2 K)	0.154	0.136–0.170	0.138–0.178	0.132–0.171	0.145–0.159	0.173–0.230	0.148–0.159	0.180–0.189	0.151
α (degree)	9.8	5.2–11	5.2–16.1	7.3–13.2	8.4–17	5–12	16.3–20	13.4–19.2	5
WWR	0.37	0.33–0.4	0.2–0.4	0.2–0.34	0.2–0.32	0.2	0.2	0.2	0.2
IT_H (W)	279	255–289	251–277	250–304	251–255	250–251	250–256	251–253	250
Shd_{Dec}	0.329	0.253–0.33	0.33	0.327–0.33	0.328–0.33	0.33	0.33	0.33	0.33
Orientation	North	North	North	North	North	North	South	South	North

The dominant thermal load in the temperate zone is space heating. Therefore, it also requires a high level of insulation and consequently lower thermal transmittance of the envelope. Interestingly, the lower limits of insulation materials and U-values are higher in the temperate—hot summer zone than temperate—warm summer zone, and the upper limits are low. The reason is that the lower limit of HDD is large, but the upper limit of HDD is small in this climate zone. Furthermore, the temperate—hot summer zone has a higher CDD. Moreover, the design variables responsible for solar gains are adjusted to minimize the solar heat gain; i.e., the ranges of WWR and IT_H decrease, and the ShdDec range increases in the temperate zone. The optimal orientation is North, the same as in the continental climate zone.

In the dry—cold zone, neither cooling nor heating is the dominant thermal load. As a result, the HDD and CDD are in the same range and have relatively low values. The insulation materials have a smaller thickness range of 0.197–0.223 m for EPS and 0.133–0.185 m for rockwool. Similarly, the U-values of the external walls and roof have relatively higher ranges of 0.165–0.184 W/m^2 K and 0.173–0.230 W/m^2 K, respectively. The window aperture angle is also smaller compared to the temperate climate. The WWR and IT_H are kept to the minimum, and ShdDec is maximized to restrict the solar gains. The optimal orientation is North in the dry—cold zone. On the other hand, the dry—hot climate is represented by a cooling-dominant thermal load and higher CDD. The optimal solution set is also quite different from that of a dry—cold climate. The thermal transmittance of the envelope is lower than the dry—cold temperate climate zones, and the window aperture angle ranges to its upper limit. The optimal orientation also changes to South in dry-hot climate. Nevertheless, other design variables are the same as in the dry—cold climate.

The tropical zone consists of cooling-dominant locations, and the CDD are above 3000 in all locations. The values of WWR, IT_H, and ShdDec follow the same trend as in other cooling-dominant climates. In Af and Aw climate zones, the EPS insulation is the highest of all climates and thus has the minimum thermal transmittance range, i.e., 0.148–0.150 W/m^2 K. However, the thermal transmittance has a comparatively higher range of 0.180–0.189 W/m^2 K. The Am climate has lesser CDD than other tropical climates and requires a relatively lower level of envelope insulation. The U-value of the external wall is 0.159 W/m^2 K, and it is 0.151 W/m^2 K for the roof. The aperture angle is 5 degrees in Am climate due to higher humidity levels throughout the year. The households are South-facing for optimum energy performance in Af and Aw climates, whereas in the Am climate the optimal orientation is North.

The simulation-based performance investigation of buildings is a well-established methodology to make appropriate decisions at the design stage. The experimental validation of building performance is time-consuming and financially infeasible. Nevertheless, the optimal values of the design parameters were compared with the previous studies for validation. Since the building design parameters are dependent on each other, the complete set of design parameters is taken for the explicit comparison. Previous studies

used different combinations of envelope parameters, and those studies were conducted for limited climate zones. However, the individual parameters were compared for different climates with the available data from previous studies.

Table 10 shows the comparison of the envelope thermal transmittance of WWR values between the current study and previous studies. Though the optimal values do not exactly match due to differences in the constraints and optimization models, the results are consistent with the previous data. The thermal transmittance in continental climates is low, and WWR has a higher value. In temperate climates, the thermal transmittance of the external walls and roof is higher than the continental region in the current study and the previous studies as well, and the difference between the optimal solutions is very small. The WWR varies between 0.2 and 0.34 in temperate climates. The recommended WWR for temperate climate zones is 0.25. The WWR has approximately the same value in the current and previous studies for temperate—hot summer climates (Cfa and Csa). The thermal transmittances of the envelope and WWR are also coherent with the previous study for the dry—hot climate (Bsk). A study conducted a parametric analysis of the household envelope for thermal transmittance between 0.2 and 0.4 W/m^2 K in different climate zones. The optimal values were found to be 0.2 (W/m^2 K); i.e., the minimum thermal transmittance in cold and hot climates. In this study, the cold and hot climates are also characterized by lower thermal transmittance of the wall and roof, as shown in Table 9. Although the comparative analysis is given for the limited climate zones, it can be asserted on the basis of the consistency between the current and previous studies that the optimization has produced conclusive results for other climates.

Table 10. Comparison of the results with previous studies.

Climate Zone	Parameters	Optimal Values	
		Current Study	Previous Studies
Dfa	U_w (W/m^2 K)	0.15	0.14 [85]
Dwa	U_w (W/m^2 K) WWR	0.154 0.4	0.12 [86] 0.31
Csb	U_w (W/m^2 K) U_r (W/m^2 K) WWR	0.185 0.171 0.2	0.16 [25] 0.16 0.29
Cfa	U_w (W/m^2 K) U_r (W/m^2 K) WWR	0.159 0.146 0.28	0.19 [87] 0.18 0.275
Csa	U_w (W/m^2 K) U_r (W/m^2 K) WWR	0.157 0.145 0.2	0.11 [25] 0.16 0.19
BSk	U_w (W/m^2 K) U_r (W/m^2 K) WWR	0.165 0.173 0.2	0.18 [25] 0.16 0.23
Temperate	WWR	0.2–0.34	0.25 [8]
Cold climate zones	U_w (W/m^2 K) U_r (W/m^2 K)	0.15–0.22 0.13–0.17	0.2 [35] 0.2
Hot climate zones	U_w (W/m^2 K) U_r (W/m^2 K)	0.15–0.18 0.15–0.23	0.2 [35] 0.2

5. Conclusions

The present work analyzes a household's passive design parameters and thermal energy demand for its dependence on the climate. TRNSYS and Python-based NSGA-III were used for bi-objective optimization of a single-family household for twenty-four cities in twenty climate zones. The design variables of the optimization problem were

insulation thickness of the envelope, window aperture angle, WWR, window shading fraction, radiation-based shading control, and orientation. Annual thermal energy demand and the investment cost of insulation were considered as the objective functions. A MCDM process was implemented through CRITIC and TOPSIS methods to find out the best solution from the PFs. Even though the optimization reduces the thermal load in all investigated climates, it is more effective in the heating-dominant regions. It is observed that the weather conditions strongly influence the passive design parameters. Moreover, the optimal solutions strictly rely on one another and do not indicate remarkable improvement in energy demand if implemented individually.

The optimization results show that thermal insulations of the envelope and WWR are the most perceptive design parameters as they determine the solar gains and transmission gains or losses of the household. In fact, the insulation material is thicker for high thermal loads. Therefore, the EPS thickness on external walls has higher ranges in continental—cold, continental—warm summer, dry—hot, and tropical climate zones. The rockwool thickness on the roof is larger in the heating-dominant locations of continental and temperate climate zones. The dry—cold climate zone is associated with mix climate conditions and requires a lower level of insulation. The windows in the south direction, which are exposed to sunlight for an extended period, try to increase the solar gains in continental and temperate climates. Similarly, the optimal orientation is North in those climates, enabling the façade with the maximum WWR to face South. On the contrary, dry—hot and tropical climate zones are characterized by cooling-dominant loads, minimum WWR, maximum Shd_{Dec}, and South (expect tropical-monsoon) as the optimal orientation.

The outcomes of this work provide comprehensive guidelines for the designers to make appropriate decisions about a household's passive design according to the climate. Previous building energy standards in the investigated locations provide only the limiting thermal transmittance values for the building envelope. These results set a benchmark for selecting energy-efficient envelope parameters and respective thermal transmittance ranges in the investigated climates, which can be applied worldwide, eliminating the traditional energy analysis process. This research study considers limited locations in each climate zone and does not perform statistical analysis for each climate. Therefore, further research should be conducted to statistically analyze these design parameters by considering more locations in each climate.

Author Contributions: Conceptualization, M.U. and G.F.; methodology, M.U.; software, M.U.; formal analysis, M.U.; writing—original draft, M.U.; supervision, G.F.; writing—review and editing, G.F. All authors have read and agreed to the published version of the manuscript.

Funding: This research received no external funding.

Institutional Review Board Statement: Not applicable.

Informed Consent Statement: Not applicable.

Data Availability Statement: The data presented in this study are available within the paper.

Conflicts of Interest: The authors declare no conflict of interest.

References

1. IEA. *Energy Technology Perspectives 2020—Special Report on Clean Energy Innovation*; IEA: Paris, France, 2020. [CrossRef]
2. Global Alliance for Building and Construction. Executive Summary of the 2020 Global Status Report for Buildings and Construction. 2020. Available online: https://globalabc.org/sites/default/files/inline-files/Buildings%20GSR_Executive_Summary%20FINAL_0.pdf (accessed on 1 November 2021).
3. Energy Information Administration (EIA). International Energy Outlook 2019. 2019. Available online: https://www.eia.gov/outlooks/ieo/pdf/ieo2019.pdf (accessed on 1 November 2021).
4. IEA. *Energy Technology Perspectives 2017*; IEA: Paris, France, 2017. Available online: https://www.iea.org/reports/energy-technology-perspectives-2017 (accessed on 1 November 2021).
5. Far, C.; Far, H. Improving energy efficiency of existing residential buildings using effective thermal retrofit of building envelope. *Indoor Built Environ.* **2019**, *28*, 744–760. [CrossRef]

6. Echenagucia, T.M.; Capozzoli, A.; Cascone, Y.; Sassone, M. The early design stage of a building envelope: Multi-objective search through heating, cooling and lighting energy performance analysis. *Appl. Energy* **2015**, *154*, 577–591. [CrossRef]
7. Yu, W.; Li, B.; Jia, H.; Zhang, M.; Wang, D. Application of multi-objective genetic algorithm to optimize energy efficiency and thermal comfort in building design. *Energy Build.* **2015**, *88*, 135–143. [CrossRef]
8. Yong, S.G.; Kim, J.H.; Gim, Y.; Kim, J.; Cho, J.; Hong, H.; Baik, Y.J.; Koo, J. Impacts of building envelope design factors upon energy loads and their optimization in US standard climate zones using experimental design. *Energy Build.* **2017**, *141*, 1–15. [CrossRef]
9. Guo, Y.; Bart, D. Optimization of design parameters for office buildings with climatic adaptability based on energy demand and thermal comfort. *Sustainability* **2020**, *12*, 3540. [CrossRef]
10. Woolley, J.; Schiavon, S.; Bauman, F.; Raftery, P. Side-by-side laboratory comparison of radiant and all-air cooling: How natural ventilation cooling and heat gain characteristics impact space heat extraction rates and daily thermal energy use. *Energy Build.* **2019**, *200*, 68–85. [CrossRef]
11. Lapinskienė, V.; Motuzienė, V.; Džiugaitė-Tumėnienė, R.; Mikučionienė, R. Impact of internal heat gains on building's energy performance. In Proceedings of the 10th International Conference on Environmental Engineering, Vilnius, Lithuania, 27–28 April 2017. [CrossRef]
12. Acar, U.; Kaska, O.; Tokgoz, N. Multi-objective optimization of building envelope components at the preliminary design stage for residential buildings in Turkey. *J. Build. Eng.* **2021**, *42*, 102499. [CrossRef]
13. Dong, Y.; Sun, C.; Han, Y.; Liu, Q. Intelligent optimization: A novel framework to automatize multi-objective optimization of building daylighting and energy performances. *J. Build. Eng.* **2021**, *43*, 102804. [CrossRef]
14. Starke, A.R.; Cardemil, J.M.; Escobar, R.; Colle, S. Multi-objective optimization of hybrid CSP+PV system using genetic algorithm. *Energy* **2018**, *147*, 490–503. [CrossRef]
15. Jalali, Z.; Noorzai, E.; Heidari, S. Design and optimization of form and facade of an office building using the genetic algorithm. *Sci. Technol. Built Environ.* **2020**, *26*, 128–140. [CrossRef]
16. Zhang, A.; Bokel, R.; van den Dobbelsteen, A.; Sun, Y.; Huang, Q.; Zhang, Q. Optimization of thermal and daylight performance of school buildings based on a multi-objective genetic algorithm in the cold climate of China. *Energy Build.* **2017**, *139*, 371–384. [CrossRef]
17. Nasruddin, N.; Sholahudin, S.; Satrio, P.; Mahlia, T.M.I.; Giannetti, N.; Saito, K. Optimization of HVAC system energy consumption in a building using artificial neural network and multi-objective genetic algorithm. *Sustain. Energy Technol. Assess.* **2019**, *35*, 48–57. [CrossRef]
18. Yang, M.-D.; Lin, M.-D.; Lin, Y.-H.; Tsai, K.-T. Multiobjective optimization design of green building envelope material using a non-dominated sorting genetic algorithm. *Appl. Therm. Eng.* **2017**, *111*, 1255–1264. [CrossRef]
19. Li, K.; Pan, L.; Xue, W.; Jiang, H.; Mao, H. Multi-Objective Optimization for Energy Performance Improvement of Residential Buildings: A Comparative Study. *Energies* **2017**, *10*, 245. [CrossRef]
20. Ferdyn-Grygierek, J.; Grygierek, K. Multi-Variable Optimization of Building Thermal Design Using Genetic Algorithms. *Energies* **2017**, *10*, 1570. [CrossRef]
21. Mayer, M.J.; Szilágyi, A.; Gróf, G. Environmental and economic multi-objective optimization of a household level hybrid renewable energy system by genetic algorithm. *Appl. Energy* **2020**, *269*, 115058. [CrossRef]
22. Ghaderian, M.; Veysi, F. Multi-objective optimization of energy efficiency and thermal comfort in an existing office building using NSGA-II with fitness approximation: A case study. *J. Build. Eng.* **2021**, *41*, 102440. [CrossRef]
23. Penna, P.; Prada, A.; Cappelletti, F.; Gasparella, A. Multi-objectives optimization of Energy Efficiency Measures in existing buildings. *Energy Build.* **2015**, *95*, 57–69. [CrossRef]
24. Rabani, M.; Madessa, H.B.; Nord, N. Achieving zero-energy building performance with thermal and visual comfort enhancement through optimization of fenestration, envelope, shading device, and energy supply system. *Sustain. Energy Technol. Assess.* **2021**, *44*, 101020. [CrossRef]
25. Ascione, F.; de Masi, R.F.; de Rossi, F.; Ruggiero, S.; Vanoli, G.P. Optimization of building envelope design for nZEBs in Mediterranean climate: Performance analysis of residential case study. *Appl. Energy* **2016**, *183*, 938–957. [CrossRef]
26. Ferrara, M.; Vallée, J.C.; Shtrepi, L.; Astolfi, A.; Fabrizio, E. A thermal and acoustic co-simulation method for the multi-domain optimization of nearly zero energy buildings. *J. Build. Eng.* **2021**, *40*, 102699. [CrossRef]
27. Chang, S.; Castro-Lacouture, D.; Yamagata, Y. Decision support for retrofitting building envelopes using multi-objective optimization under uncertainties. *J. Build. Eng.* **2020**, *32*, 101413. [CrossRef]
28. Delgarm, N.; Sajadi, B.; Delgarm, S. Multi-objective optimization of building energy performance and indoor thermal comfort: A new method using artificial bee colony (ABC). *Energy Build.* **2016**, *131*, 42–53. [CrossRef]
29. Moghtadernejad, S.; Chouinard, L.E.; Mirza, M.S. Multi-criteria decision-making methods for preliminary design of sustainable facades. *J. Build. Eng.* **2018**, *19*, 181–190. [CrossRef]
30. Iwaro, J.; Mwasha, A.; Williams, R.G.; Zico, R. An Integrated Criteria Weighting Framework for the sustainable performance assessment and design of building envelope. *Renew. Sustain. Energy Rev.* **2014**, *29*, 417–434. [CrossRef]
31. Xu, C.; Ke, Y.; Li, Y.; Chu, H.; Wu, Y. Data-driven configuration optimization of an off-grid wind/PV/hydrogen system based on modified NSGA-II and CRITIC-TOPSIS. *Energy Convers. Manag.* **2020**, *215*, 112892. [CrossRef]

32. Babatunde, M.; Ighravwe, D. A CRITIC-TOPSIS framework for hybrid renewable energy systems evaluation under techno-economic requirements. *J. Proj. Manag.* **2019**, *4*, 109–126. [CrossRef]
33. Salameh, T.; Sayed, E.T.; Abdelkareem, M.A.; Olabi, A.G.; Rezk, H. Optimal selection and management of hybrid renewable energy System: Neom city as a case study. *Energy Convers. Manag.* **2021**, *244*, 114434. [CrossRef]
34. Zhao, J.; Du, Y. Multi-objective optimization design for windows and shading configuration considering energy consumption and thermal comfort: A case study for office building in different climatic regions of China. *Sol. Energy* **2020**, *206*, 997–1017. [CrossRef]
35. Harkouss, F.; Fardoun, F.; Biwole, P.H. Passive design optimization of low energy buildings in different climates. *Energy* **2018**, *165*, 591–613. [CrossRef]
36. Naji, S.; Aye, L.; Noguchi, M. Multi-objective optimisations of envelope components for a prefabricated house in six climate zones. *Appl. Energy* **2021**, *282*, 116012. [CrossRef]
37. Harkouss, F.; Fardoun, F.; Biwole, P.H. Multi-objective optimization methodology for net zero energy buildings. *J. Build. Eng.* **2018**, *16*, 57–71. [CrossRef]
38. Delgarm, N.; Sajadi, B.; Delgarm, S.; Kowsary, F. A novel approach for the simulation-based optimization of the buildings energy consumption using NSGA-II: Case study in Iran. *Energy Build.* **2016**, *127*, 552–560. [CrossRef]
39. Boverket. *The National Board of Housing, Building and Planning's Building Regulations*; BBR 18, BFS 2011:26; The Swedish National Board of Housing, Building and Planning: Stockholm, Sweden, 2011.
40. Mikulits, R.; Wolfgang, T. *OIB-Directives 6: Energy Saving and Thermal Protection*; Austrian Institute of Construction Engineering: Wien, Austria, 2015.
41. Longo, S.S.; Cellura, M.; Cusenza, M.A.; Guarino, F.; Marotta, I. Selecting insulating materials for building envelope: A life cycle approach. *Tec. Ital.-Ital. J. Eng. Sci.* **2021**, *65*, 312–316. [CrossRef]
42. Bienvenido-Huertas, D.; Oliveira, M.; Rubio-Bellido, C.; Marín, D. A comparative analysis of the international regulation of thermal properties in building envelope. *Sustainability* **2019**, *11*, 5574. [CrossRef]
43. Mahboob, M.; Rashid, T.U.; Amjad, M. Assessment of Energy Saving Potential in Residential Sector of Pakistan through Implementation of NEECA and PEC Building Standards. In Proceedings of the 2019 15th International Conference on Emerging Technologies (ICET), Peshawar, Pakistan, 2–3 December 2019; pp. 1–6.
44. Government of Dubai. *A Practice Guide for Building a Sustainable Dubai*; Dubai Green Building System: Dubai, United Arab Emirates, 2020.
45. Building and Construction Authority. *Code for Environmental Sustainability of Buildings*; Building and Construction Authority: Singapore, 2012.
46. Bureau of Energy Efficiency. *Energy Conservation Building Code*; Bureau of Energy Efficiency: Sewa Bhawan, India, 2017.
47. ASHRAE. Standard 90.2-2018, Energy Efficient Design of Low-Rise Residential Buildings. 2018. Available online: https://www.ashrae.org/news/esociety/newly-revised-standard-90-2-includes-new-performance-specifications-more (accessed on 1 November 2021).
48. Pacific Northwest National Laboratory. *Country Report on Building Energy Codes in China*; US Department of Energy: Washington, DC, USA, 2009.
49. Ramin, H.; Karimi, H. Optimum envelope design toward zero energy buildings in Iran. In *E3S Web of Conferences, 6–9 September 2020*; EDP Sciences: Tallinn, Estonia, 2020; p. 16004. [CrossRef]
50. Council, A. Energy efficiency building standards in Japan. *Acesso Em Março* **2007**, 1–9. Available online: http://www.asiabusinesscouncil.org/docs/BEE/papers/BEE_Policy_Japan.pdf (accessed on 1 November 2021).
51. Hansen, C.F.; Hansen, M.L. *Executive Order on the Publication of the Danish Building Regulations 2015 (BR15)*; The Danish Transport and Construction Agency: Copenhagen, Denmark, 2015.
52. Vogdt, F.U.; Walsdorf-Maul, M.; Schwabe, K.; Schaudienst, F.; Baumbach, A. Comparison between calculating methods of energy saving regulations and their economic efficiency. *Czas. Techniczne. Bud.* **2012**, *109*, 423–430.
53. Britain, G. *The Building Regulations 2010: Conservation of Fuel and Power: Approved Document L1A*; NBS: Chicago, IL, USA, 2014.
54. Bordier, R.; Rezaï, N. *Implementing the Energy Performance of Buildings Directive-EPBD Implementation in France*; EASME: Saint-Josse-ten-Noode, Belgium, 2018.
55. Bruke, R.V.; Gil, M.S.; Gonzalez, D.J.; Rodriguez, J.S. *Guía de Aplicación del DB-HE 2019—CTE*; Ministry of Transport, Mobility and Urban Agenda and Urban Agenda: Madrid, Spain, 2020.
56. Dott, R.; Ruschenburg, J.; Ochs, F.; Bony, J.; Haller, M. The Reference Framework for System Simulation of the IEA SHC Task 44/HPP Annex 38—Part B: Buildings and Space Heat Load. 2013. Available online: http://task44.iea-shc.org/data/sites/1/publications/T44A38_Rep_C1_B_ReferenceBuildingDescription_Final_Revised_130906.pdf (accessed on 1 November 2021).
57. TRANSSOLAR Energietechnik. Multizone Building Modeling with Type56 and TRNBuild. In Trnsys 18 Documantation; 2017; Volume 5. Available online: http://www.trnsys.com/ (accessed on 1 November 2021).
58. Parsons, R. (Ed.) *ASHRAE Handbook—Fundamentals*; American Society of Heating Refrigerating and Air-Conditioning Engineers: Atlanta, GA, USA, 1997.
59. ASHRAE Project Committee 90.1, Schedules and Internal Loads for Appendix C. Available online: https://web.ashrae.org/90_1files/ (accessed on 1 November 2021).
60. Parsons, R. (Ed.) *ASHRAE Handbook—Fundamentals*; American Society of Heating Refrigerating and Air-Conditioning Engineers: Atlanta, GA, USA, 2001.

61. Widén, J.; Lundh, M.; Vassileva, I.; Dahlquist, E.; Ellegård, K.; Wäckelgård, E. Constructing load profiles for household electricity and hot water from time-use data-Modelling approach and validation. *Energy Build.* **2009**, *41*, 753–768. [CrossRef]
62. Verein Deutscher Ingenieure. *VDI 4655—Reference Load Profiles of Single-Family and Multi-Family Houses for the Use of CHP Systems*; Verein Deutscher Ingenieure: Düsseldorf, Germany, 2008.
63. The Energy Informatics Group. PRECON Pakistan Residential Electricity Consumption Dataset. 2019. Available online: https://opendata.com.pk/dataset/precon-pakistan-residential-electricity-consumption-dataset (accessed on 1 November 2021).
64. Almohanna, I. Solar Dcathlon Middle East, Team KSU: Project Manual. 2019. Available online: https://www.solardecathlonme.com/2018/storage/reports/KSU-Project-manual.pdf (accessed on 1 November 2021).
65. Gupta, P.; Zan, T.T.T.; Dauwels, J.; Ukil, A. Flow-Based Estimation and Comparative Study of Gas Demand Profile for Residential Units in Singapore. *IEEE Trans. Sustain. Energy* **2019**, *10*, 1120–1128. [CrossRef]
66. Garg, A.; Shukla, P.R.; Maheshwari, J.; Upadhyay, J. An assessment of household electricity load curves and corresponding CO_2 marginal abatement cost curves for Gujarat state, India. *Energy Policy* **2014**, *66*, 568–584. [CrossRef]
67. Kubota, T.; Surahman, U.; Higashi, O. A comparative analysis of household energy consumption in Jakarta and Bandung. In Proceedings of the 30th International PLEA Conference: Sustainable Habitat for Developing Societies, Choosing the Way Forward, Gujarat, India, 16–18 December 2014; Volume 2, pp. 260–267.
68. Wang, H.; Fang, H.; Yu, X.; Liang, S. How real time pricing modifies Chinese households' electricity consumption. *J. Clean. Prod.* **2018**, *178*, 776–790. [CrossRef]
69. Hakimi, S.M. Multivariate stochastic modeling of washing machine loads profile in Iran. *Sustain. Cities Soc.* **2016**, *26*, 170–185. [CrossRef]
70. Shiraki, H.; Nakamura, S.; Ashina, S.; Honjo, K. Estimating the hourly electricity profile of Japanese households—Coupling of engineering and statistical methods. *Energy* **2016**, *114*, 478–491. [CrossRef]
71. Trotta, G. An empirical analysis of domestic electricity load profiles: Who consumes how much and when? *Appl. Energy* **2020**, *275*, 115399. [CrossRef]
72. Zimmermann, J.-P.; Evans, M.; Griggs, J.; King, N.; Harding, L.; Roberts, P.; Evans, C. Household Electricity Survey: A Study of Domestic Electrical Product Usage. 2012. Available online: https://www.gov.uk/government/uploads/system/uploads/attachment_data/file/208097/10043_R66141HouseholdElectricitySurveyFinalReportissue4.pdf (accessed on 1 November 2021).
73. Csoknyai, T.; Legardeur, J.; Akle, A.A.; Horváth, M. Analysis of energy consumption profiles in residential buildings and impact assessment of a serious game on occupants' behavior. *Energy Build.* **2019**, *196*, 1–20. [CrossRef]
74. Alberini, A.; Prettico, G.; Shen, C.; Torriti, J. Hot weather and residential hourly electricity demand in Italy. *Energy* **2019**, *177*, 44–56. [CrossRef]
75. Policy, S.E.; Francisco, D.; Freire, M.; Ferreira, C. Residential Sector Energy Consumption at the Spotlight: From Data to Knowledge. 2017. Available online: http://alteracoesclimaticas.ics.ulisboa.pt/wp-content/teses/2017JoaoGouveia.pdf (accessed on 1 November 2021).
76. Kuusela, P.; Norros, I.; Weiss, R.; Sorasalmi, T. Practical lognormal framework for household energy consumption modeling. *Energy Build.* **2015**, *108*, 223–235. [CrossRef]
77. Xiong, J.; Tzempelikos, A. Model-based shading and lighting controls considering visual comfort and energy use. *Sol. Energy* **2016**, *134*, 416–428. [CrossRef]
78. Bre, F.; Silva, A.S.; Ghisi, E.; Fachinotti, V.D. Residential building design optimisation using sensitivity analysis and genetic algorithm. *Energy Build.* **2016**, *133*, 853–866. [CrossRef]
79. ASHRAE. Standard 90.1-2019, Energy Standard for Buildings Except Low-Rise Residential Buildings. 2019. Available online: https://www.ashrae.org/technical-resources/bookstore/standard-90-1 (accessed on 1 November 2021).
80. Kottek, M.; Grieser, J.; Beck, C.; Rudolf, B.; Rubel, F. World Map of the Köppen-Geiger climate classification updated. *Meteorol. Z.* **2006**, *15*, 259–263. [CrossRef]
81. Benítez-Hidalgo, A.; Nebro, A.J.; García-Nieto, J.; Oregi, I.; del Ser, J. jMetalPy: A Python framework for multi-objective optimization with metaheuristics. *Swarm Evol. Comput.* **2019**, *51*, 100598. [CrossRef]
82. Li, H.; Deb, K.; Zhang, Q.; Suganthan, P.N.; Chen, L. Comparison between MOEA/D and NSGA-III on a set of many and multi-objective benchmark problems with challenging difficulties. *Swarm Evol. Comput.* **2019**, *46*, 104–117. [CrossRef]
83. Insulation Materials. Available online: https://www.obi.de/baustoffhalle/daemmstoffe/c/233#/ (accessed on 5 April 2021).
84. ASHRAE. Standard 55, Thermal Environmental Conditions for Human Occupancy. 2020. Available online: https://www.ashrae.org/technical-resources/bookstore/standard-55-thermal-environmental-conditions-for-human-occupancy (accessed on 1 November 2021).
85. Geng, Y.; Han, X.; Zhang, H.; Shi, L. Optimization and cost analysis of thickness of vacuum insulation panel for structural insulating panel buildings in cold climates. *J. Build. Eng.* **2021**, *33*, 101853. [CrossRef]
86. Wang, R.; Lu, S.; Feng, W. Impact of adjustment strategies on building design process in different climates oriented by multiple performance. *Appl. Energy* **2020**, *266*, 114822. [CrossRef]
87. Ascione, F.; Bianco, N.; Mauro, G.M.; Napolitano, D.F. Building envelope design: Multi-objective optimization to minimize energy consumption, global cost and thermal discomfort. Application to different Italian climatic zones. *Energy* **2019**, *174*, 359–374. [CrossRef]